Naval Surface Warfare Center
Carderock Division
West Bethesda, MD 20817-5700

NSWCCD-50-TR-2008/066 November 2008

Hydromechanics Department Report

Design of the ONR AxWJ-2 Axial Flow Water Jet Pump

by

Thad J. Michael
Seth D. Schroeder
Alan J. Becnel

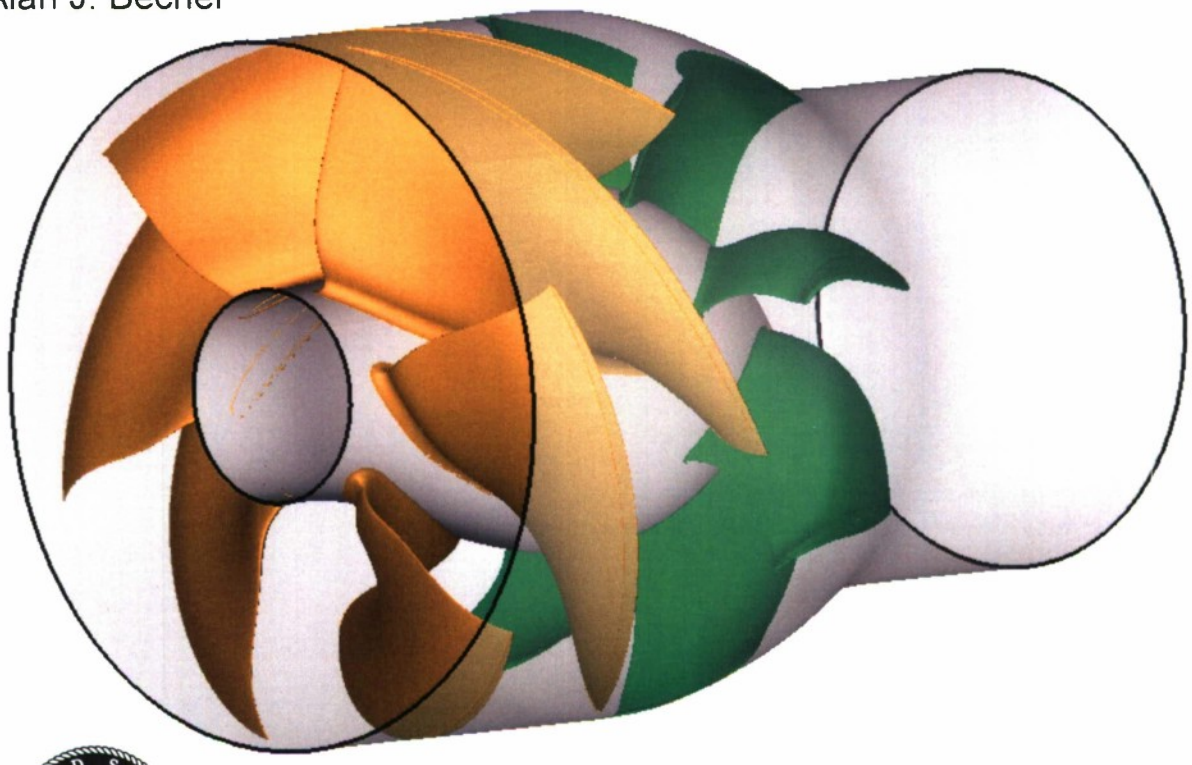

NSWCCD-50-TR-2008/066 Design of the ONR AxWJ-2 Axial Flow Water Jet Pump

REPORT DOCUMENTATION PAGE

Form Approved
OMB No. 0704-0188

1. REPORT DATE *(DD-MM-YYYY)*	2. REPORT TYPE	3. DATES COVERED *(From - To)*
November 2008	Final	January 2008 - August 2008

4. TITLE AND SUBTITLE
Design of the ONR AxWJ-2 Axial Flow Water Jet Pump

5a. CONTRACT NUMBER

5b. GRANT NUMBER

5c. PROGRAM ELEMENT NUMBER

6. AUTHOR(S)
Thad J. Michael
Seth D. Schroeder
Alan J. Becnel

5d. PROJECT NUMBER

5e. TASK NUMBER

5f. WORK UNIT NUMBER
08-1-5800-240-10

7. PERFORMING ORGANIZATION NAME(S) AND ADDRESS(ES) AND ADDRESS(ES)

Resistance and Propulsion Division, Code 5800
Naval Surface Warfare Center Carderock Division
9500 Macarthur Boulevard
West Bethesda, MD 20817-5700

8. PERFORMING ORGANIZATION REPORT NUMBER

NSWCCD-50-TR-2008/066

9. SPONSORING / MONITORING AGENCY NAME(S) AND ADDRESS(ES)
Office of Naval Research
875 North Randolph St.
Arlington, VA 22203

10. SPONSOR/MONITOR'S ACRONYM(S)

11. SPONSOR/MONITOR'S REPORT NUMBER(S)

12. DISTRIBUTION / AVAILABILITY STATEMENT
Distribution statement A:
Approved for public release. Distribution unlimited.

13. SUPPLEMENTARY NOTES

14. ABSTRACT

An axial flow water jet pump has been designed for model testing. The design is based on the requirements of a notional high speed ship. The potential flow blade method PBD-14/MTFLOW was used for the blade shaping. The Reynolds-Averaged Navier-Stokes codes CFX and Fluent were used to evaluate the designs.

This model pump was specifically designed for model testing in the NSWCCD 36 Inch Water Tunnel, the Johns Hopkins University water tunnel, and the Rolls-Royce Hydrodynamic Research Centre water tunnel. Each water tunnel has unique requirements.

This report describes the design of the pump, including the methods and philosophy used in the shaping of the hub, casing, rotor, and stator. A comparison of the predictions from the three methods is included.

The predicted full scale pump efficiency is 92%; the predicted model scale efficiency is 90%. It is recommended that this pump be manufactured and tested at all three facilities.

15. SUBJECT TERMS
PROPULSOR, HYDRODYNAMICS

16. SECURITY CLASSIFICATION OF:			17. LIMITATION OF ABSTRACT	18. NUMBER OF PAGES	19a. NAME OF RESPONSIBLE PERSON
					Thad J. Michael
a. REPORT	b. ABSTRACT	c. THIS PAGE			19b. TELEPHONE NUMBER
UNCLASSIFIED	UNCLASSIFIED	UNCLASSIFIED	SAR	60	(301) 227-5831

(THIS PAGE INTENTIONALLY LEFT BLANK)

CONTENTS

NOMENCLATURE vi

ABBREVIATIONS vii

ABSTRACT 1

ADMINISTRATIVE INFORMATION 1

INTRODUCTION 1

DESIGN REQUIREMENTS 2

PARAMETRIC STUDY 2

DESIGN FOR TESTING 3

DESIGN METHODS 3

PBD-14/MTFLOW 4

ANSYS CFX 4

ANSYS FLUENT 5

HUB AND CASING DESIGN 6

HUB 6

CASING 7

BLADE DESIGN 7

PHILOSOPHY 7

ROTOR DESIGN 8

STATOR DESIGN 10

EXPERIENCE WITH RANS CODES 11

ROTOR AND STATOR GEOMETRY 12

GEOMETRIC DETAILS 12

PREDICTED PERFORMANCE 13

FUTURE WORK 14

CONCLUSIONS 14

ACKNOWLEDGEMENTS 15

APPENDIX A: GEOMETRY TABLES 41

HUB AND CASING GEOMETRY 41

ROTOR GEOMETRY 43

STATOR GEOMETRY 47
REFERENCES **51**

FIGURES

1. Overview of design process. 17
2. Passage geometry and mean axial velocity ratio. 17
3. Section generation curves for non-conical blade geometry. 18
4. Sectional pressure distributions for early design showing suction peak at leading edge. 19
5. Rotor pressure side maximum principal stress distribution in psi. 20
6. Rotor radial deflection at full power in inches. 20
7. Rotor spanwise circulation distribution. 21
8. Rotor chordwise loading distribution (PBD-14). 21
9. Rotor suction side pressure distribution from CFX. 22
10. Rotor sectional pressure distributions. 23
11. Stator trailing edge pitch angle. 24
12. Stator spanwise circulation distribution. 24
13. Velocity at a plane downstream of stator. 25
14. Stator skew distributions for pressure comparison. 25
15. Stator chordwise pressure distributions, +15 and -15 degrees of skew (CFX). 26
16. Stator pressure side maximum principal stress distribution in psi. 27
17. Stator chordwise loading distribution (PBD-14). 27
18. Stator sectional pressure distributions. 28
19. Stator suction side pressure distribution from CFX. 29
20. Rotor spanwise chord distribution. 29
21. Rotor spanwise thickness distribution. 30
22. Rotor spanwise skew distribution. 30
23. Rotor spanwise rake distribution. 31
24. Rotor spanwise pitch distribution. 31
25. Rotor spanwise camber distribution. 32
26. Rotor section shapes. 33
27. Stator spanwise chord distribution. 34
28. Stator spanwise thickness distribution. 34

29. Stator spanwise skew distribution. 35
30. Stator spanwise rake distribution. 35
31. Stator spanwise pitch distribution. 36
32. Stator spanwise camber distribution....36
33. Stator section shapes. 37
34. Rotor trailing edge....38
35. Stator trailing edge. 38
36. Stator tip fillet, section at x/R=1.35. 39
36. Stator tip fillet....39
37. Performance of a 12 inch (304.8 mm) pump....40
38. Performance of a 70 inch (1778 mm) pump....40

TABLES

1. Predicted model scale performance....13
2. Predicted full scale performance. 14
A-1. Hub and casing geometry....41
A-2. Rotor spanwise geometry. 43
A-3. Rotor section shape, 0% span....44
A-4. Rotor section shape, 20% span....44
A-5. Rotor section shape, 40% span....45
A-6. Rotor section shape, 60% span....45
A-7. Rotor section shape, 80% span....46
A-8. Rotor section shape, 100% span....46
A-9. Stator spanwise geometry. 47
A-10. Stator section shape, 0% span. 48
A-11. Stator section shape, 20% span. 48
A-12. Stator section shape, 40% span. 49
A-13. Stator section shape, 60% span. 49
A-14. Stator section shape, 80% span. 50
A-15. Stator section shape, 100% span. 50

NOMENCLATURE

c	Chord length
C_P	Pressure coefficient = $p/(\frac{1}{2}\rho V^2)$
D	Diameter
f	Camber
g	Gravitational constant
G	Non-dimensional circulation
h	Coordinate orthagonal to chordwise
H	Head
H*	Normalized head = $gH/(n^2D^2)$
k	Kinetic energy of turbulence
K_Q	Torque coefficient = torque/$(\rho n^2 D^5)$
P	Power
p	Pressure
P*	Normalized power = $P/(\rho n^3 D^5)$
Q	Volumetric flow rate
Q*	Normalized flow rate = $Q/(nD^3)$
r	Local radius
r_r	Degree of reaction
R	Pump inlet radius
s	Distance along chord
t	Thickness
T_R	Radial component of deflection
V	Velocity
V_0	Inlet velocity
V_T	Tangential velocity
V_X	Axial velocity
w	Wake fraction
x	Axial coordinate
y	Coordinate normal to a surface
y^+	Defined by $\frac{y(\lvert\tau_w\rvert/\rho_w)^{1/2}}{\nu_w}$ where the subscript w indicates the value at the wall
Δ	Change

ε	Dissipation rate of turbulence
η_P	Pump efficiency
ν	Kinematic viscosity
ρ	Mass density
$\sigma_{P\,Max}$	Maximum principal stress
τ	Shear stress
ω	Rotation speed

ABBREVIATIONS

ASCII	Americal standard code for information interchange
CCDoTT	Center for the Comercial Development of Transportation Technology
HRC	Hydrodynamic Research Centre
JHU	Johns Hopkins University
JVR_A	Jet velocity ratio, using wake velocity
LDV	Laser Doppler velocimetry
MIT	Massachusetts Institute of Technology
NACA	National Advisory Committee for Aeronautics
NSWCCD	Naval Surface Warfare Center, Carderock Division
NURBS	Non-uniform rational b-spline
ONR	Office of Naval Research
PIV	Particle image velocimetry
RANS	Reynolds-averaged Navier-Stokes
RPM	Revolutions per minute
SST	Shear stress transport
WJOPTIM	Water Jet optimization program

(THIS PAGE INTENTIONALLY LEFT BLANK)

ABSTRACT

An axial flow water jet pump has been designed for model testing. The design is based on the requirements of a notional high speed ship. The potential flow blade design method PBD-14/MTFLOW was used for the blade shaping. The Reynolds-Averaged Navier-Stokes codes CFX and Fluent were used to evaluate the designs.

This model pump was specifically designed for model testing in the NSWCCD 36 Inch Water Tunnel, the Johns Hopkins University water tunnel, and the Rolls-Royce Hydrodynamic Research Centre water tunnel. Each water tunnel has unique requirements.

This report describes the design of the pump, including the methods and philosophy used in the shaping of the hub, casing, rotor, and stator. A comparison of the predictions from the three methods is included.

The predicted model scale efficiency is 90%. The predicted efficiency of a notional full scale pump is 92%. It is recommended that this pump be manufactured and tested at all three facilities.

ADMINISTRATIVE INFORMATION

This work was sponsored by Dr. Ki-Han Kim, Office of Naval Research (ONR), code 333. The work was conducted by the Naval Surface Warfare Center, Carderock Division (NSWCCD), Hydromechanics Department, Resistance and Propulsion Division (Code 5800) and the Seakeeping Division (Code 5500) under job order number 08-1-5800-240-10.

INTRODUCTION

This report describes the design of an axial flow water jet pump for research and development. The objective of this design was to improve the water jet design capabilities at NSWCCD and to create a new geometry from model testing. The pump was sized to power a notional high speed ship. The detail design was performed using a combination of inviscid and viscous computational analysis methods. The report describes, in detail, the difficulties and solutions encountered using these methods while developing this design.

DESIGN REQUIREMENTS

This pump was designed for model scale testing. The model scale requirement was for a 12 inch (304.8 mm) pump operating at 2000 rpm.

To make this design relevant, a notional high speed ship was assumed. General Electric LM-2500 gas turbine drive was assumed with a delivered power of 27,500 hp (20.5 MW) at a speed of 50 knots. An assumed full scale inlet diameter of 67 inches (1700 mm) was used. A wake fraction, (1-w), of 0.90 and a thrust deduction, (1-t), of 1.09 were assumed based on previous experience with water jet propulsion.

PARAMETRIC STUDY

A brief parametric study was conducted to select the design point. The parametric study used the program WJOPTIM[1] to investigate a range of jet velocity ratios and flow coefficients. The program assumes a uniform inlet axial velocity distribution and a constant circulation distribution on the rotor. The program calculates the minimum pump diameter by maximizing the axial velocity for a given flow rate while ensuring that the static pressure is sufficient to avoid complete thrust breakdown. An empirical method is used to estimate pump efficiency and the jet velocity ratio is used to compute the jet efficiency.

A flow coefficient, Q*, of 0.85 was selected for the design point with a notional jet velocity to wake speed ratio, JVR_A, of 1.5.

With the selected flow coefficient of 0.85, the model scale rpm and diameter resulted in a flow rate of 28.3 ft^3/sec (0.802 m^3/s). With an expected pump efficiency of about 0.88, this was expected to produce a head rise of about 76.6 ft (23.3 m). Any improvement in efficiency would result in a greater head rise.

If this pump were designed for an actual ship and the efficiency was higher than expected once the pump design was complete, the nozzle diameter would be adjusted to maintain the selected flow coefficient. The ship would achieve a higher speed at the installed power than predicted by the initial parametric calculations. However, this pump was primarily designed for model testing.

[1] Described in a report with limited distribution.

DESIGN FOR TESTING

This pump was designed for testing in three facilities. Each of these facilities has unique capabilities and also special requirements. Testing in three facilities will result in the most complete collection of data for a water jet pump assembled to date.

The NSWCCD 36 Inch Water Tunnel has a water jet testing bellmouth with a 12 inch (304.8 mm) flange for the pump inlet. The tunnel relies upon the pump nozzle and a downstream orifice to provide back pressure. Flow rate is further controlled by the water tunnel impeller. A camera mounted on the drive shaft allows visualization of the cavitating area. A laser Doppler velocimetry (LDV) system allows detailed time-averaged measurements of the flow field. To fit a window for LDV measurements between the rotor and the stator, a one inch (25.4 mm) cylindrical region between the rotor and the stator was required.

The Rolls-Royce Hydrodynamic Research Centre (HRC) pump loop requires a pump with a 200 mm (7.874 in) inlet diameter and a 140 mm (5.512 in) exit diameter. The outflow is routed through a pump which controls the mass flow rate through the water jet pump. This facility has been used extensively for commercial water jet designs. A greater range of torque and headrise data can be collected at this facility than the 36 Inch Water Tunnel because of the direct control of the mass flow rate.

The Johns Hopkins University (JHU) water tunnel requires a pump with a 12 inch (304.8 mm) inlet flange. The entire pump is machined out of acrylic. The tunnel is filled with an index of refraction matched fluid so that particle image velocimetry (PIV) measurements can be made through the blades and in the tip gap. The index-matched fluid is a 62%-64% by weight solution of NaI in water. This fluid has a specific gravity of 1.8 and kinematic viscosity of 1.1×10^{-6} m^2/s, very close to that of water. A 0.020 inch (0.51 mm) tip gap size was selected to allow at least 10 PIV measurement points through the thickness of the gap. In the absence of this requirement, the gap size would be the smallest permitted by mechanical considerations and computed blade deflection.

DESIGN METHODS

The design was completed using three primary tools: PBD-14/MTFLOW, CFX, and Fluent. These tools were used to design the hub, casing, and blade shapes. Also, NEiNastran was used for structural analysis of the blades. Figure 1 shows an overview of the design process. The hub and casing were designed first, then the rotor, then the stator. The process looped backwards whenever a part needed to be redesigned. Design calculations were performed with Reynolds

number based on the assumed 67 inch (1700 mm) full scale inlet diameter. Model scale RANS calculations were later used to predict model scale performance.

PBD-14/MTFLOW

PBD-14 is a vortex lattice propeller code from the Massachusetts Institute of Technology (MIT) [1]. MTFLOW is an axisymmetric Euler solver also from MIT [2]. These two programs can be coupled to solve the flow through a water jet pump [3]. PBD-14 solves for the three-dimensional flow around the blades, and passes the tangential induced velocities to MTFLOW. MTFLOW uses the tangential velocities and work from the blades to update the flow field and returns the updated flow field to PBD-14.

In design mode, PBD-14 solves the velocities on the blade surface for a given loading distribution. This may result in velocities that pass through the blades. BSHAPE [4], developed at NSWCCD, uses these velocities and the blade geometry to compute the required change in pitch and camber to satisfy the kinematic boundary condition. This new geometry is then used with PBD-14 and BSHAPE and the process is repeated until the given loading distribution and the kinematic boundary condition are both satisfied.

To design the rotor, PBD-14, MTFLOW, and BSHAPE are iterated until the blade shape and flow field converge. The solution is generally well converged within 15 iterations. During these iterations, a notional stator is used to completely cancel tangential velocities downstream of the rotor.

The stator may be designed simultaneously with the rotor, or the rotor may be analyzed while the stator is designed. For both the rotor and stator a 21-by-20 vortex-lattice mesh was used, with uniform spacing in the spanwise direction and cosine spacing in the chordwise direction.

ANSYS CFX

CFX is a commercially available Reynolds-Averaged Navier-Stokes code from ANSYS used to analyze the viscous performance of turbomachinery. CFX is broken into modules to perform the required tasks for the performance estimate. The hub, shroud and blade profiles were provided from PBD-14 in the form of ASCII files. These ASCII files were read into ANSYS-Turbogrid to generate the rotor and stator structured grids. The grid size and spacing was adjusted to get a y^+ spacing from all surfaces of less than 2 for use with the SST turbulence model [5]. This grid topology was saved in a script file for use during each geometry update so that each grid has essentially the same size and spacing.

ANSYS-CFX Pre was used to setup the physics of the calculation. The working fluid, RPM, steady-state or transient, non-cavitating or cavitating, massflow and other boundary conditions, etc. are setup in this module. Two types of calculations were performed, rotor only calculations and rotator and stator together calculations using a mixing plane between the two frames of reference.

ANSYS-CFX Solver was used to solve the RANS equations for this water jet pump. The solver execution time was typically 15-20 minutes for a rotor only calculation and about 3-4 hours for a rotor-stator calculation using a Dell M90 portable workstation.

ANSYS-CFX Post was used to export the required parameters for the next geometry iteration with PBD-14. These included torque, headrise, pressure distributions on both the blade surfaces and hub and shroud surfaces, and rotor and overall pump efficiency.

ANSYS FLUENT

Fluent [6] is a commercially available Reynolds-Averaged Navier-Stokes code capable of analyzing the performance of a water jet pump design. The mesh for Fluent is created using Ansys IcemCFD Hexa. ICEM is used to create a structured topology domain that defines a hexahedral meshing scheme. Because the geometry varies slightly between design iterations, a script can automatically generate the structured topology.

The geometry is defined using surfaces, curves, and points. This geometry is created using a NCBLADE [7,8] input file, an axisymmetric definition for the casing, and an axisymmetric definition for the hub. The NCBLADE input file is an output of the PBD-14 design process. The surfaces are created by rotating the hub and casing definitions axially, and by setting NCBLADE to output a NURBS surface. The curves and points are both generated by rotating and scaling data from the Tecplot output of NCBLADE.

Once the geometry is imported to ICEM, the topology domain is divided with a top-down approach. The blocking is fitted to the geometry by splitting the blocks at certain points. Every vertex that is created by a split in the blocking is given an imported point to snap to. The block edges that reside on the hub or casing surfaces are fit to the surface. The block edges not on surfaces are given an imported curve to snap to. Once the topology is fitted to the geometry, ICEM writes out a Fluent input mesh. The mesh size is approximately 375,000 cells for the rotor only, and 750,000 cells for the rotor and stator together. This mesh size allows for sufficient boundary layer resolution with the use of Fluent's wall functions. The y^+ values average 50-60 on the surfaces, and a sufficient number of cells fill the tip gap.

A steady state pressure based solver is used in Fluent to analyze the pump design. The k-ε turbulence model is used with enhanced wall functions. A single blade passage is analyzed in a rotating reference frame with rotationally periodic boundaries. Because of the different number of rotor and stator blades, the periodic rotation angles are not the same. This is overcome by the use of a mixing-plane model. The mixing-plane is defined between the rotor and stator and the solution is circumferentially averaged by area across the plane to go from the rotor to the stator domain.

The solution process is streamlined by interpolating the previous design iteration's solution on to the new problem. This allows for a convergence time of one hour or less when the 750,000 cell mesh is solved using seven processors.

The typical results of interest are the pressure distributions on the blade surface, the net torque, the head rise, and the velocity profiles downstream of each blade row. The visual data sets are exported in Tecplot format. Fluent has been previously used for water jet calculations as reported by Brewton [9]. The results are also compared with predications from CFX, which has been used in previous water jet pump designs [10].

HUB AND CASING DESIGN

As the rotor and stator designs evolve, it is necessary to update the hub and casing design to reflect the axial length of the rotor and stator. The initial axial lengths of the rotor and stator were based on chord lengths from previous designs and quickly replaced by more refined values.

HUB

The radius of three points on the rotor hub can be readily determined: the leading edge of the blades, the trailing edge of the blades, and the tail cone.

The leading edge of the rotor blades should be at a radius of about 0.3R to limit blockage and the additional twist that would be needed at smaller radii. Keeping the passage area as large as possible helps to keep the static pressure up. It is also advantageous for the slope of the hub to be near zero at the leading edge of the rotor to keep the passage area as large as possible as long as possible. However, if the hub shape changes too quickly it will create a stress concentration.

The radius of the trailing edge of the rotor can be determined from the degree of reaction, or reaction ratio. It can be shown that when there is no tangential velocity in the inflow, the degree of reaction is:

$$r_r = 1 - \frac{V_T}{2\omega r} \qquad (1)$$

where V_T is the tangential velocity at the hub at the trailing edge and r is the hub radius at the trailing edge [11]. The degree of reaction must be greater than 0.50 so that the tangential velocity will be less than the rotational speed of the blade. This conclusion would lead to a local blade pitch of zero degrees.

The radius must approach zero at the tail end of the hub. A small truncated or rounded area is preferable to a pointed cone because it will be stronger and resist hub vortex formation. The axial length of the hub is determined by the required chord length of the rotor and stator plus the distance between blades and some hub length downstream of the stator. The hub is extended downstream of the stator to reduce losses by preventing the flow from separating immediately.

CASING

The first part of the casing, in way of the rotor, is simple on an axial flow water jet pump: it is cylindrical. Downstream of the rotor, the casing is shaped to avoid any sudden changes in passage area. It is best to delay as much of the contraction as possible until at least midchord in the stator, because the contraction of the passage reduces the static pressure on the blades. Once the stator converts some swirl to pressure, the passage area can be contracted without reducing the static pressure below that at the leading edge of the stator. Once the flow has left the stator blades, the passage should contract as quickly as possible to meet atmospheric pressure since any extra length will lead to extra viscous losses. However, the convex curvature of the nozzle must be monitored for low static pressure that could lead to cavitation. Figure 2 shows the mean velocity change based on the passage area.

In this case, due to special model test considerations, the casing radius continues to be cylindrical for one inch downstream of the rotor for a twelve inch diameter pump. This is to allow a window to be fitted for LDV access.

BLADE DESIGN

PHILOSOPHY

The objective of the design of the rotor and stator blades was to achieve the design torque with adequate cavitation margin and maximum efficiency. Therefore, areas of minimum pressure were changed, through changes in loading distribution, chord length, rake, or skew to raise the pressure of that region of the blade. In areas where the static pressure was higher than required, the loading distribution was changed or the chord length was reduced to improve efficiency. Consequently, the blades are designed to have relatively constant pressure distributions on the

suction side. Similar to propellers with advanced blade sections, these blades are expected to begin to cavitate all at once. These blades are also expected to delay thrust breakdown relative to blades with less carefully designed pressure distributions because these blades have a lower inception pressure.

The blade sections were designed on arbitrary axisymmetric surfaces, similar to stream tubes. The hub and tip axisymmetric surfaces were defined by the geometry of the hub and casing. The intermediate surfaces were defined at a constant fraction of the distance between the hub and casing. Figure 3 shows the axisymmetric surfaces on which the final design is based.

The NACA 16 chordwise thickness distribution was used for the rotor blades. This thickness distribution is common in propellers and resulted in good performance here. In future designs, the chordwise thickness could be optimized for off design conditions cavitation performance as it is for modern propellers.

ROTOR DESIGN

Typical waterjet pump rotors have four to six blades, some have as many as seven. With six blades, the chord-to-diameter ratio of this rotor falls within the range of 0.5 to 1.0. Fewer blades may reduce blockage, leading to a higher minimum pressure, but requiring an increase in the chord length and length of the pump. More blades could reduce the length of the pump, but would be likely to also reduce the minimum pressure. For this design, six blades produced acceptable minimum pressures with a reduced length relative to the CCDoTT pump [10].

To design the blades with BSHAPE, the camber must be set to zero at some chordwise position. That position must be the same one used to define rake and skew. Otherwise, without anything anchoring it to a smooth curve, the blade develops unwanted wiggles in the spanwise direction. For this rotor design, the 75% chord position was used for the reference curve. Thus, the camber at the leading and trailing edges is not zero, nor is it the same at the leading edge and trailing edge. The 75% chord position was determined to be better than the 50% chordwise position based on the overall appearance of the blade. The location of the reference line is shown in Figure 3.

Upon analyzing the initial rotor designs with CFX, it was found that the torque predicted by CFX was 15% lower than the torque predicted by PBD-14. Also, the sectional pressure distributions showed that the sections were not aligned for shock free entry. As shown in Figure 4, there was a suction peak on the pressure side over the entire span. A similar error, a suction peak on the pressure side, was also found with the previous ONR AxWJ-1 rotor, which was designed without the benefit of RANS [12].

The shock free entry problem was solved by applying an empirical correction. The blade was designed in PBD-14/MTFLOW using an advance coefficient, J, 12% higher than the target J value. RANS calculations confirmed that this resulted in shock free entry. The design value of K_Q for PBD-14/MTFLOW was adjusted by the analytical amount due to the J shift, for this case $(1/1.12)^2$.

With the adjusted advance coefficient, the torque predicted by CFX and Fluent was 5% greater than the target torque. This was corrected by applying an empirical correction factor. The design torque used in PBD-14/MTFLOW was 95% of the target torque. This resulted in a rotor blade with shock free entry and the correct torque.

Rotor skew and rake near the root was selected to make the blade stand out from the hub as much as possible. This was adjusted as the design progressed. It is undesirable for manufacturing when the angle between the blade and the hub becomes small due to the changing pitch and camber of the blade combined with the rake and skew.

Away from the root, rake was selected to position the blade within the desired portion of the passage. The rotor is raked forward, where the passage cross section area is larger. Skew was selected to minimize the amount of radial deflection under load. Because water jet rotor tip gaps are relatively small, the deflection of the blade under load could potentially cause the blade to contact the casing. During the design process, finite element calculations were used to ensure the blades would not touch the casing under load. Nickel-Aluminum-Bronze was assumed, with a full scale diameter of 67 inches (1700 mm). A full scale size was used because stress does not scale linearly with the pump size. Figure 5 shows the distribution of principal stress on the pressure side of the rotor blade at full power. The maximum principal stress is 11,100 psi (76.5 MPa). Figure 6 shows the radial deflection at full power.

The most efficient spanwise loading for the rotor would be constant circulation across the span. However, that results in a very twisted blade due to a large pitch and camber change between the root and tip. Too much twist can result in a difficult blade to manufacture and can increase the radial component of the deflection under load. A design with less load at the hub than at the tip will have less twist. It is important to avoid any rapid changes in the spanwise loading distribution since these will result in undesirable rapid changes in pitch and camber. Figure 7 shows the spanwise loading of the rotor.

The chordwise loading distributions were manipulated to produce relatively constant pressures on the suction side. Figure 8 shows the chordwise loading distribution on the rotor at three radii. After the chordwise loading distributions were determined, the chord lengths were adjusted so that the minimum pressure would be similar, and above the cavitation limit, at all radii. Modest changes in the circulation distribution were also used to equalize the minimum

pressures. Figure 9 is a contour plot of the suction side pressures predicted by CFX. It shows that the minimum pressure is similar across a range of radii.

The sectional pressure distributions computed by PBD-14, CFX, and Fluent are shown in Figure 10. At 10% and 50% span, the pressure distributions from PBD-14 and the RANS codes agree well. However, at 90% span, the RANS codes predict a lower pressure than PBD-14. The pressure at the tip is lower than anywhere else on the blade. Despite multiple attempts, it was not possible to further improve the pressure at the tip using the current design method. It is not clear why the PBD-14 results deviate from the CFX and Fluent results more at the tip than at other radii. The difference may be due to the tip gap which is modeled in RANS but not in PBD-14.

STATOR DESIGN

Blade number selection for the stator was difficult because the rotor has six blades. Unfortunately, with a six bladed stator, there is no reasonable stator blade number which will avoid both unsteady thrust and side force interactions. To minimize unsteady forces due to blade number interaction, a higher number of blades would be preferred, but would also reduce chord length and increase blockage. The eight-bladed stator has an almost constant chord-to-diameter ratio of approximately 0.4; an eleven bladed stator would reduce the chord-to-diameter ratio to approximately 0.3. The radius of curvature between the nozzle and the stator casing was already leading to pressures below the minimum on the stator blades and if the casing was shortened it would result in a smaller radius of curvature and lower pressures. For this reason, a reduced stator chord length would not result in a reduced pump length. It was decided to use eight stator blades to reduce manufacturing costs.

For the stator design, the camber was set to zero at midchord. Therefore the camber at the leading and trailing edges was the same. This produced an aesthetically pleasing blade.

An empirical correction to PBD-14 was also necessary for the stator design. The tangential velocity produced by the rotor in the RANS analysis need to be reduced by 5% for PBD-14 design calculations. With this correction, RANS analysis of the stator showed shock free entry. In practice, this was achieved by increasing the tangential velocity from the rotor design calculations by 10%. As stated earlier, the torque from PBD-14 was about 15% less than RANS, so when the PBD-14 tangential velocity was increased by 10% it was then 5% less than RANS.

The spanwise loading distribution on the stator was adjusted through trial and error to minimize the swirl downstream of the stator, as predicted by PBD-14. The angle of the stator trailing edges were also monitored. Near the root, the stator trailing edge should point almost straight downstream, with increasing turning approaching the tip, as shown in Figure 11. This

method was found to predict swirl cancellation with reasonable accuracy. Figure 12 shows the stator spanwise circulation distribution. Figure 13 compares the swirl downstream of the stator as predicted by PBD-14, CFX, and Fluent. The residual swirl is less than 5% of the mean inlet velocity. The energy loss represented by this tangential velocity is negligible compared with the total energy in the jet. The strong positive tangential velocity at the hub is presumably due to boundary layer effects and the tapered end of the hub. It has been suggested that this could be eliminated with a long, straight trailing edge strake on the stator blades.

The stator blade has positive skew. Positive skew was found to increase the static pressure at the stator tips relative to an equal amount of negative skew. Figure 14 compares skew distributions of positive and negative 15 degrees and the resulting pressure distributions are shown in Figure 15. Positive skew appears to be less desirable for unsteady forces, since the stator blades will lean in the same direction as the rotor trailing edges. However, unsteady force calculations were not used in this design. Unsteady force calculations are recommended for future designs.

The minimum thickness for the stator was set at 4.5% of chord length to allow an adequate leading edge radius to minimize cavitation during anticipated inflow variations. Finite element analysis was used to examine stress levels. It was assumed that the rotor thrust bearing would be located outside of the pump, therefore the stator blades would not have to carry that load. The thickness was increased near the root and tip to minimize stress concentrations and allow room for pins in the stator tips which where planned for both of the 12 inch models. The maximum principal stress distribution on the pressure side of the stator is shown in Figure 16. The maximum principal stress is 8100 psi (55.8 MPa).

Again, the chordwise loading distributions were manipulated to produce relatively constant pressures on the suction side. Figure 17 shows the chordwise loading distribution on the stator at three radii. The resulting pressure distributions computed by PBD-14, CFX, and Fluent are shown in Figure 18. Figure 19 is a contour plot of the suction side pressures predicted by CFX. It shows that the minimum pressure is similar across a range of radii. Despite multiple attempts, it was not possible to further improve the pressure at the root using the current design method. It is theorized that the image model used in PBD-14 does not work well for this region because it is highly non-cylindrical.

EXPERIENCE WITH RANS CODES

The two RANS codes used in this design, CFX and Fluent, returned similar results. Both could produce useful rotor evaluations in under an hour when the designers were available to pass

the geometry and post process the results without delay. An effort was made to make the exchange of geometry and results as easy as possible through the use of bash shell scripts and custom programs for translating the geometry. Fillets were not modeled and trailing edges were treated as flat with square edges.

RANS codes should be used in the design of all future water jet pumps. Although they could not be used to determine the blade shape based on a pressure distribution as PBD-14 could, they filled the critical role of calibrating the PBD-14 calculations. Because of the limitations of potential flow for internal flow pumps, a design performed without RANS cannot be expected to perform properly until a larger experience base has been accumulated. At a minimum, RANS should always be used to confirm the design.

ROTOR AND STATOR GEOMETRY

The rotor has six blades. The spanwise geometry is plotted in Figures 20-25. The chordwise section shapes are shown in Figure 26. The rotor has a NACA 16 chordwise thickness distribution. The expanded area ratio, EAR, is 1.947.

The stator has eight blades. The spanwise geometry is plotted in Figures 27-32. The chordwise section shapes are shown in Figure 33. The stator has a NACA 16 chordwise thickness distribution. The expanded area ratio, EAR, is 1.287.

The geometry of both blade rows and the hub and casing is tabulated in Appendix A.

GEOMETRIC DETAILS

TRAILING EDGE DETAILS

Propellers generally have anti-singing trailing edge bevels. However, these features are not commonly applied to water jet blades. In the design process, the trailing edges were modeled in RANS as flat surfaces. The objective of the trailing edge detail design was to remove the sharp edges which would be difficult to fillet and replace them with more rounded shapes without changing the loading on the blade.

The rotor trailing edge thickness is 10% of the maximum section thickness at the root and 15% at the tip. The trailing edge is flat, with a small radius on each side, as shown in Figure 34.

The stator trailing edge thickness is 10% of the maximum section thickness at the root and 13% at the tip. Because the stator trailing edge is much thinner than the rotor trailing edge, a trailing edge similar to the rotor was not practical, the radius would be too small or the flat would be negligible. So, a radius was applied to the trailing edge. The trailing edge radius on the stator is approximately equal to the radius applied to the edges on either side of the flat rotor trailing

edge. Figure 35 shows the stator trailing edge. The rounded trailing edge increases the risk of the vortex shedding that leads to singing. However, because trailing edge bevels are not commonly used on water jet pumps, it is believed that singing has not been a problem.

FILLETS

The root of the rotor and stator blades was filleted with a radius that is one-third of the local section thickness, as commonly used for propeller blades. At the leading and trailing edges, the root fillet decreases to a minimum radius which is maintained constant as the fillet wraps around the leading or trailing edge.

The fillet for the tip of the stator blade was generated using a custom program. This fillet is not a radius and does not blend into the casing. This is because the stator will be manufactured separately from the casing; the blade cannot meet the casing with zero thickness. A section at x/R=1.35 is shown in Figure 36. The stator tip fillet at the leading edge and trailing edge is shown in Figure 37.

PREDICTED PERFORMANCE

Fluent was used to compute head rise, torque, and efficiency for a 12 inch (304.8 mm) model pump operating at 2000 rpm. These quantities are plotted in Figure 38 for a range of flow rates and tabulated in Table 1. The efficiency of the model pump is predicted to be 90% at the design flow coefficient of 0.85.

Table 1. Predicted model scale performance.

Q^*	H^*	K_Q	η_P
0.595	2.87	0.322	0.827
0.680	2.82	0.335	0.904
0.765	2.56	0.338	0.914
0.808	2.40	0.337	0.909
0.850	2.24	0.335	0.898
0.893	2.08	0.330	0.890
0.935	1.92	0.324	0.872
1.020	1.52	0.307	0.770

For water jet pumps, there is a larger difference between model scale and full scale performance than with propellers. To assess full scale performance, CFX was used to compute head rise, torque, and efficiency for a pump with a 67 inch (1700 mm) inlet. These quantities are plotted in Figure 39 for a range of flow rates. The head rise and efficiency include nozzle losses.

These quantities are tabulated in Table 2. The efficiency of a 70 inch pump is predicted to be 92% at the design flow rate.

Table 2. Predicted full scale performance.

Q^*	H^*	K_Q	η_P
0.597	2.94	0.325	0.820
0.682	2.82	0.334	0.898
0.767	2.59	0.338	0.926
0.810	2.44	0.337	0.924
0.852	2.29	0.335	0.918
0.895	2.13	0.330	0.906
0.938	1.96	0.324	0.879
1.023	1.55	0.306	0.776

FUTURE WORK

Further development of PBD-14 is needed to improve upon the image model and add a tip gap model for design and analysis. Professor Justin Kerwin of MIT is working on these areas and has written a research version of the code which includes a paneled hub and casing [4]. He is currently working on a tip gap model. These features should be incorporated into PBD-14.

It is known that smaller tip gap sizes improve efficiency. Rounding the tip may reduce the pressure difference across the tip of the rotor and improve efficiency or reduce cavitation. It may be worthwhile to investigate potential efficiency benefits from altering the tip shape.

In a future designs, the effect of non-uniform inflow could be evaluated at the design stage. This could be accomplished with RANS calculations or PROPCAV-WJ [13] which could be used to compute a cavitation bucket. The thickness and chord distributions could then be optimized as they are for advanced blade sections.

Hydrodynamic calculations with the fillets have not been made. The effect of the fillets, and ways to optimize fillets and strakes should be investigated.

CONCLUSIONS

An axial flow water jet pump has been successfully designed for the Office of Naval Research to use for further water jet research testing. A 12 inch (304.8 mm) model pump is expected to have an efficiency of 90% at the design flow coefficient, 0.85, and 2000 rpm. A

pump with a 70 inch (1778 mm) inlet would have an efficiency of 92% at the design flow coefficient.

It is recommended that this pump be manufactured at model scale with a 12 inch (304.8 mm) inlet diameter and tested both in the NSWCCD 36 Inch Water Tunnel and in the Johns Hopkins University index matched flow facility. It is also recommended that a pump with a 200 mm (7.874 in) inlet be manufactured and tested at the Rolls Royce Hydrodynamic Research Centre.

ACKNOWLEDGEMENTS

The authors would like to thank Dr. Ki-Han Kim of ONR for funding this effort. Stuart Jessup, Scott Black, Stephen Neely, Michael Wilson, and Martin Donelly provided valuable insight and suggestions throughout the design.

(THIS PAGE INTENTIONALLY LEFT BLANK)

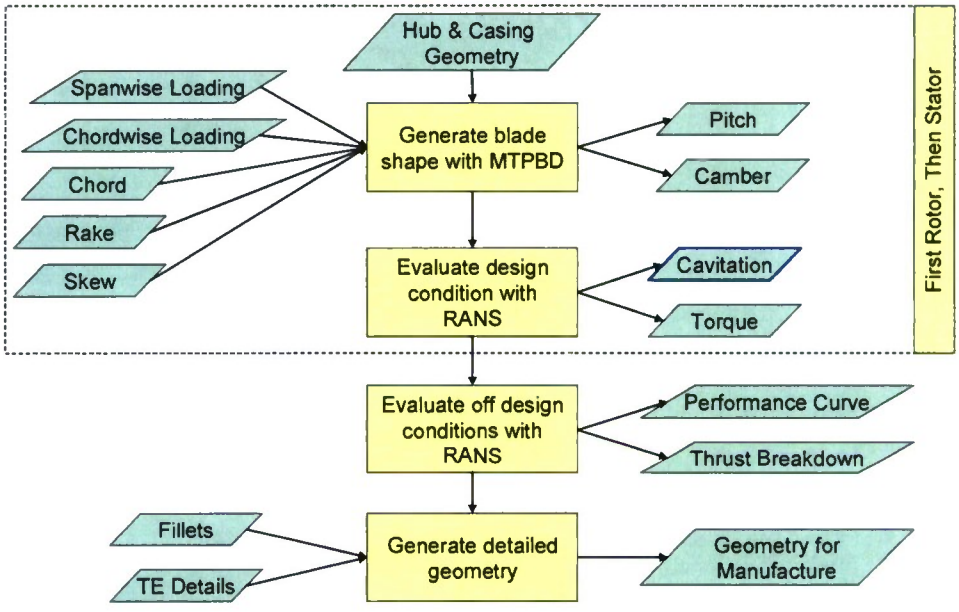

Figure 1. Overview of design process.

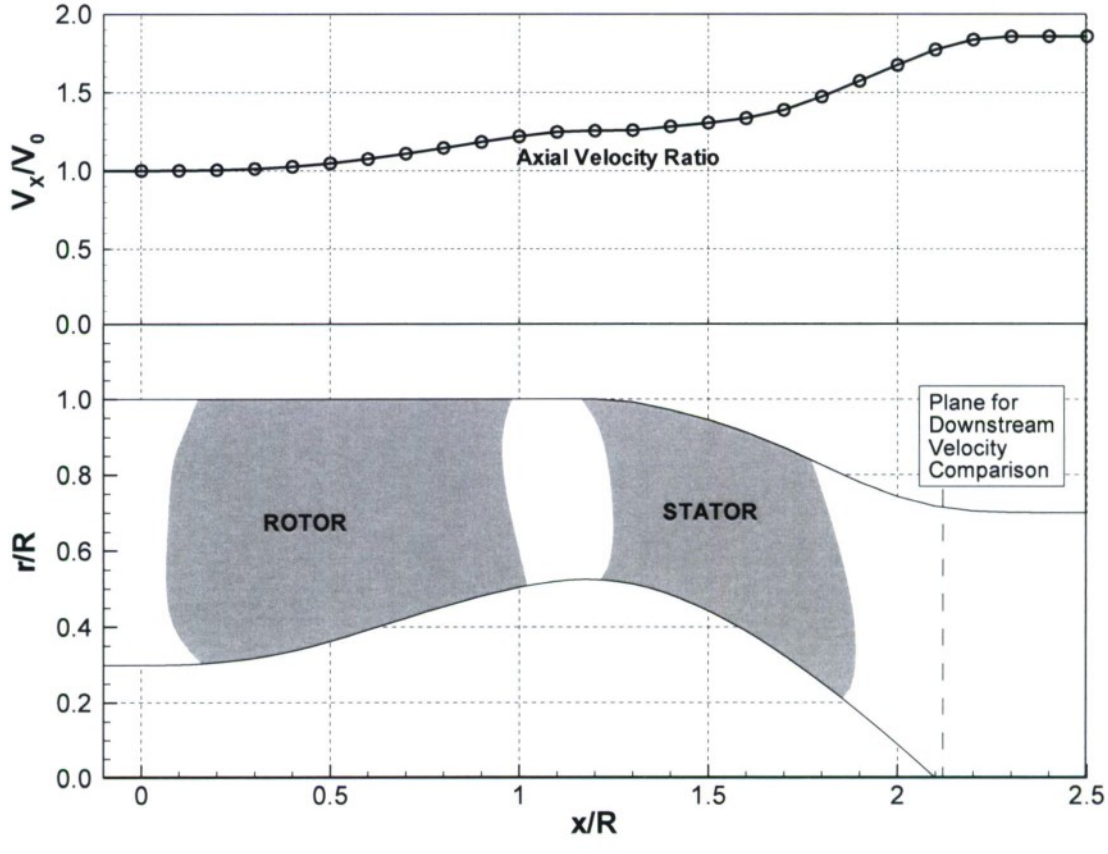

Figure 2. Passage geometry and mean axial velocity ratio.

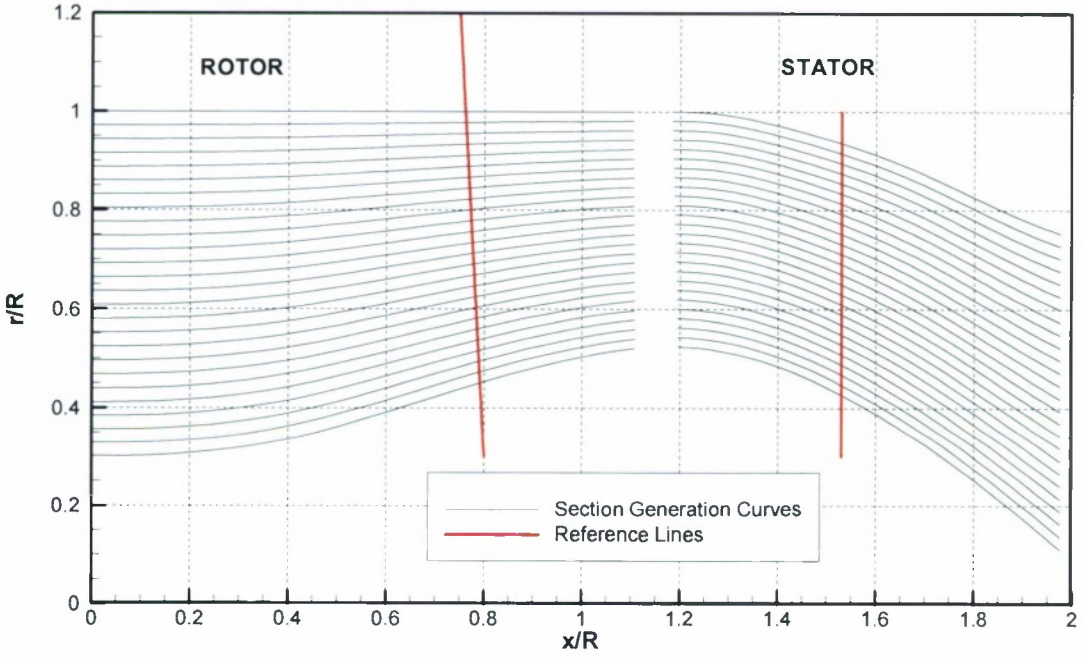

Figure 3. Section generation curves for non-conical blade geometry.

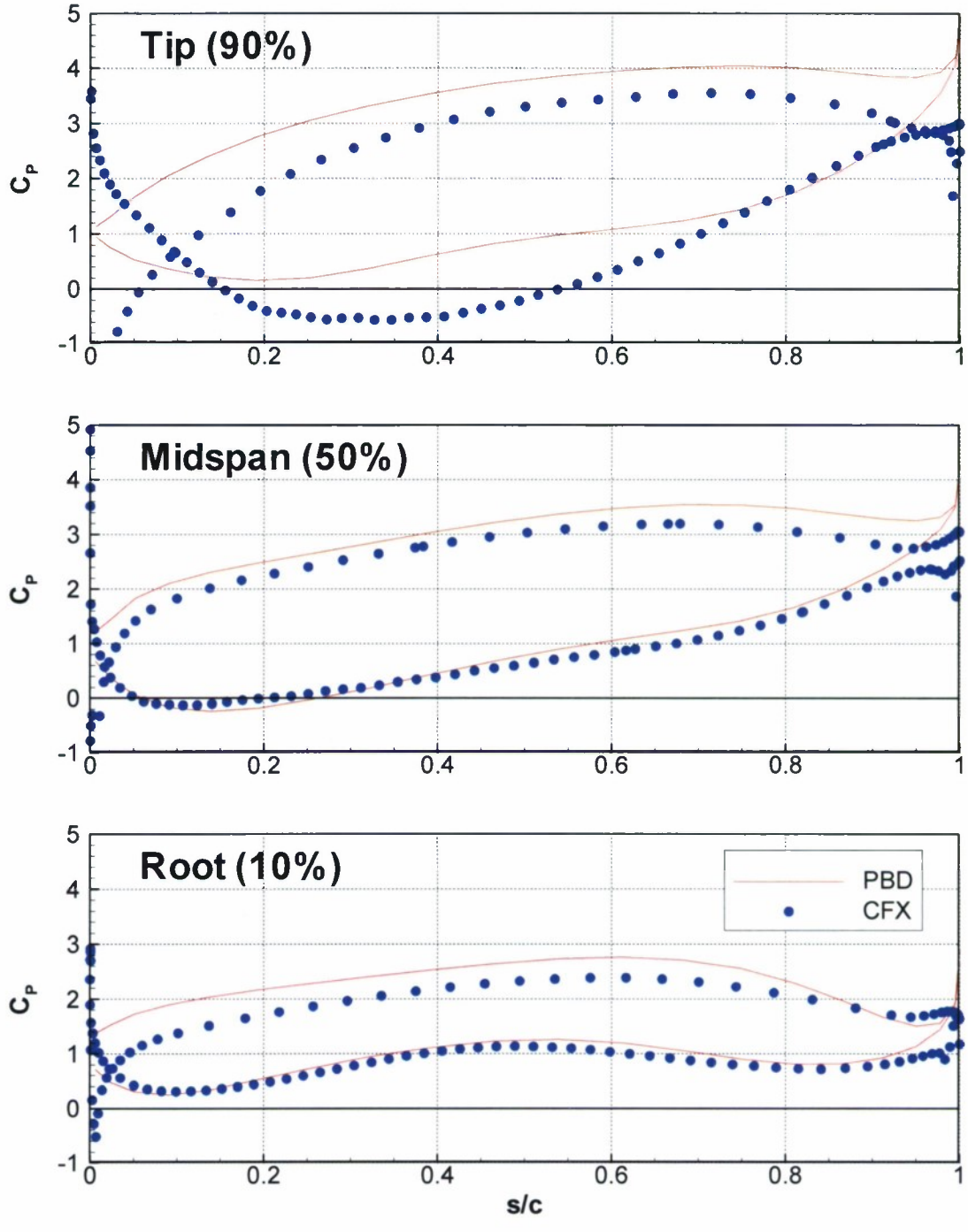

Figure 4. Sectional pressure distributions for early design showing suction peak at leading edge.

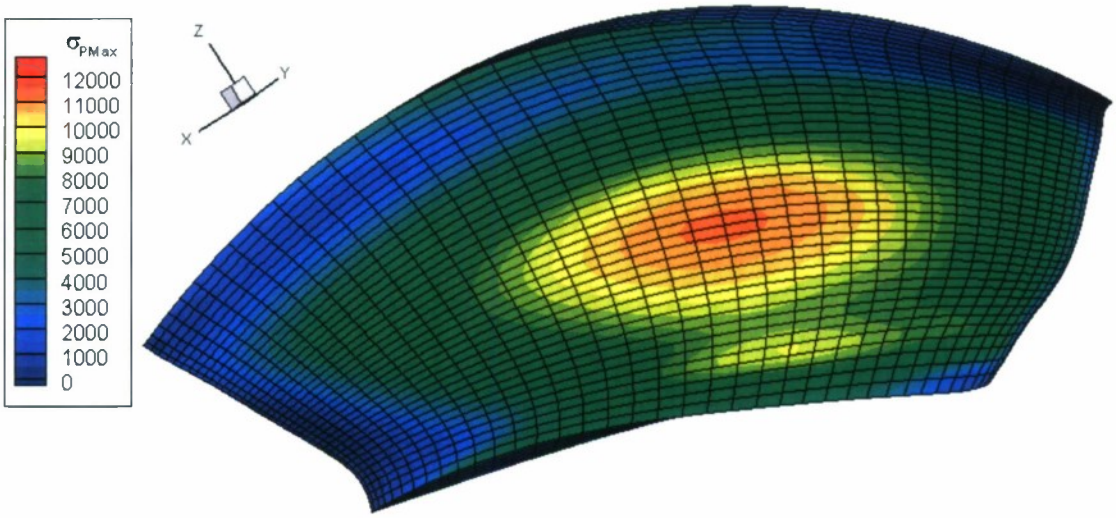

Figure 5. Rotor pressure side maximum principal stress distribution in psi.

Assumes 67 inch (1700 mm) diameter pump, nickel-aluminum-bronze.

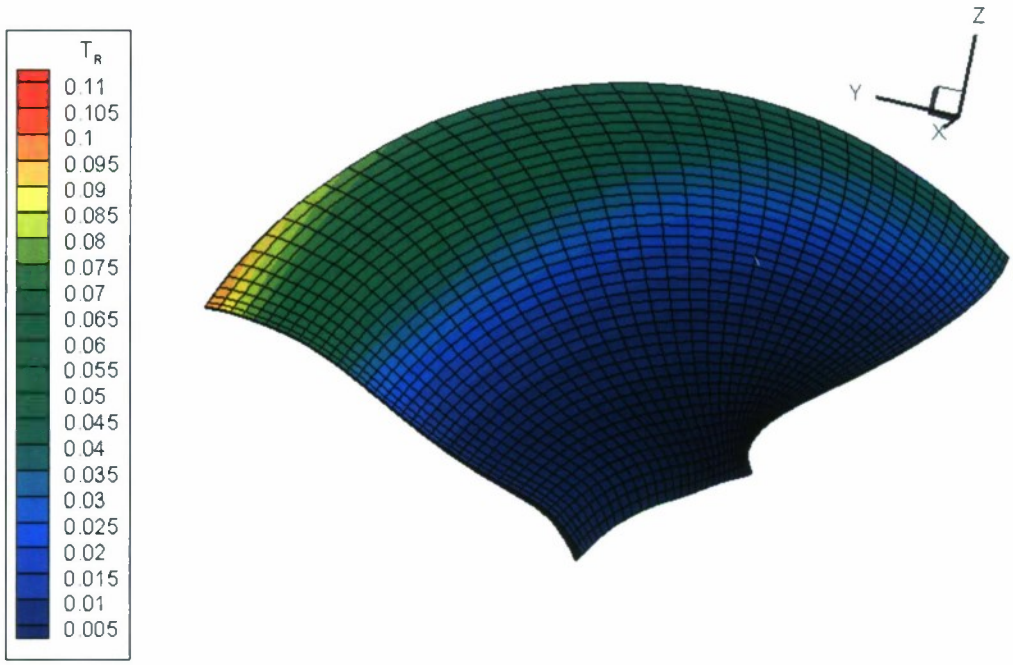

Figure 6. Rotor radial deflection at full power in inches.

Assumes 67 inch (1700 mm) diameter pump, nickel-aluminum-bronze.

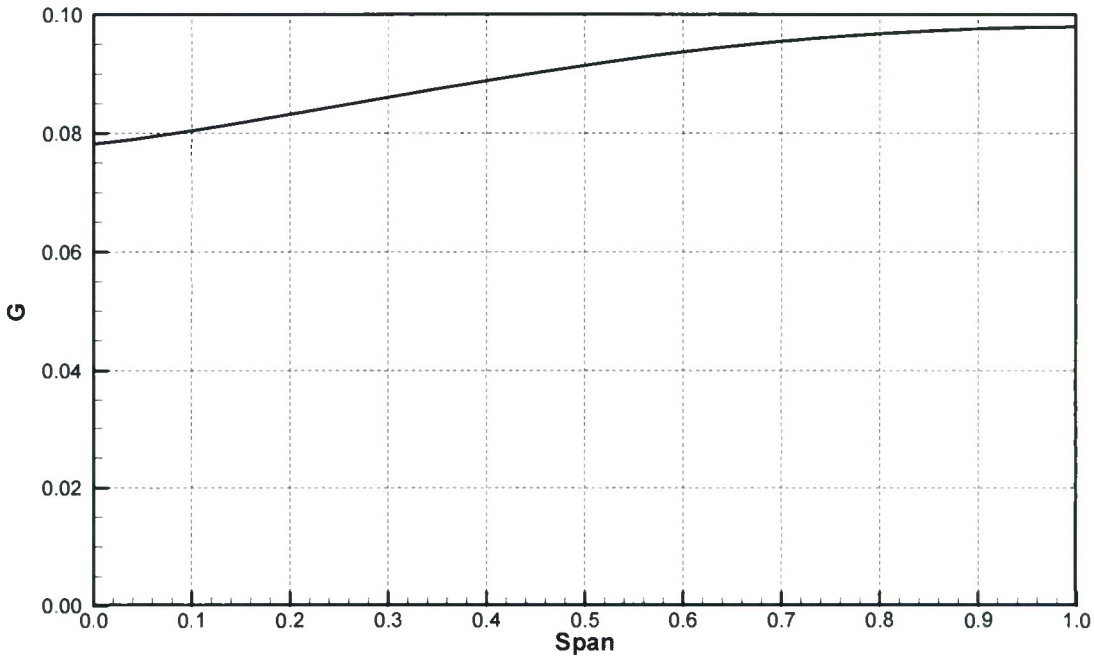

Figure 7. Rotor spanwise circulation distribution.

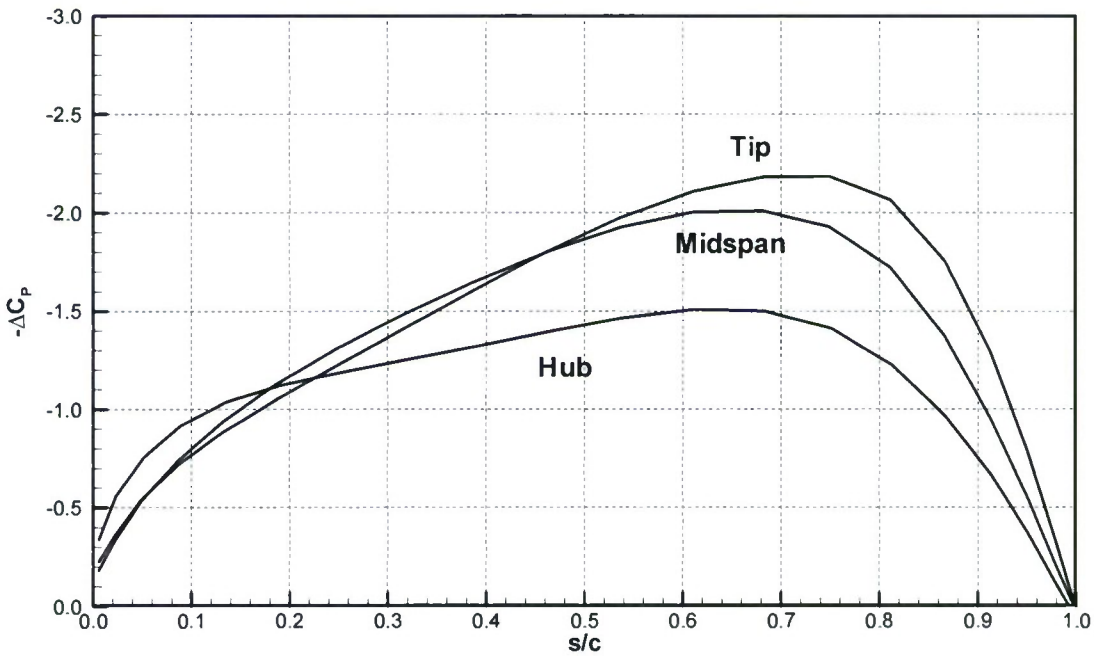

Figure 8. Rotor chordwise loading distribution (PBD-14).

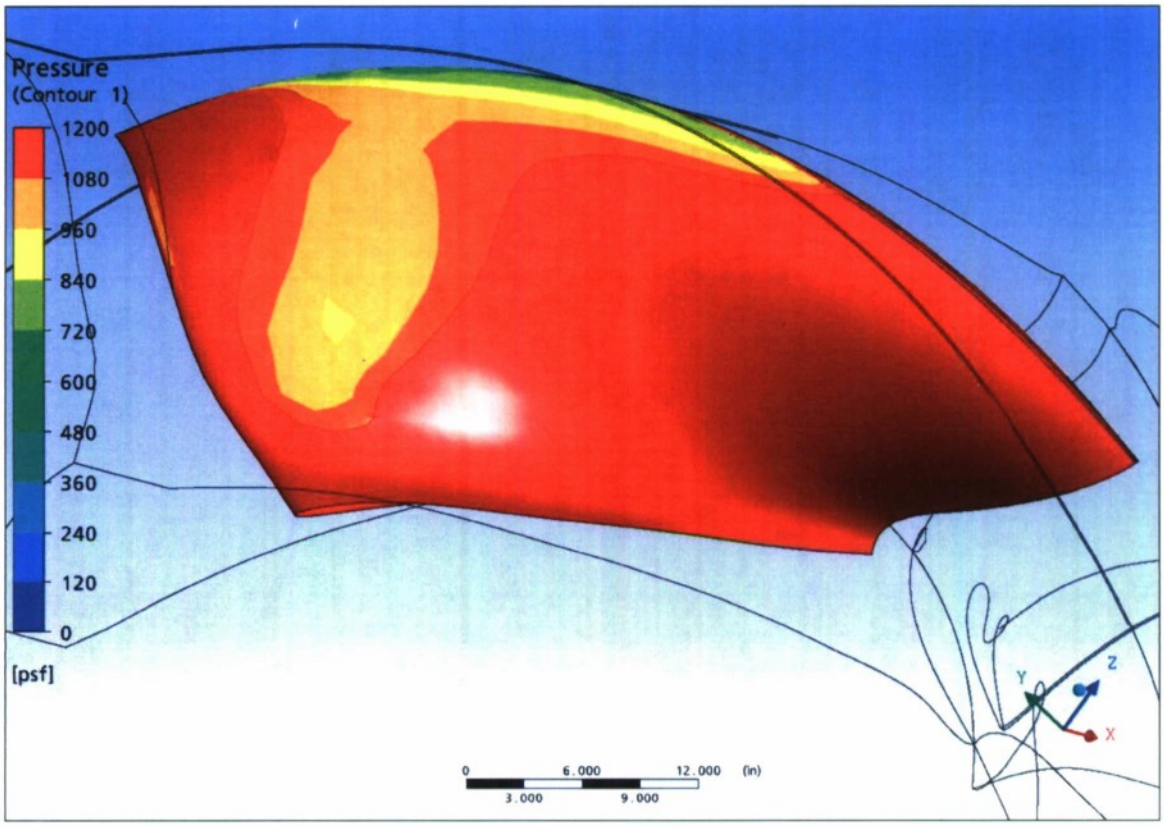

Figure 9. Rotor suction side pressure distribution from CFX.

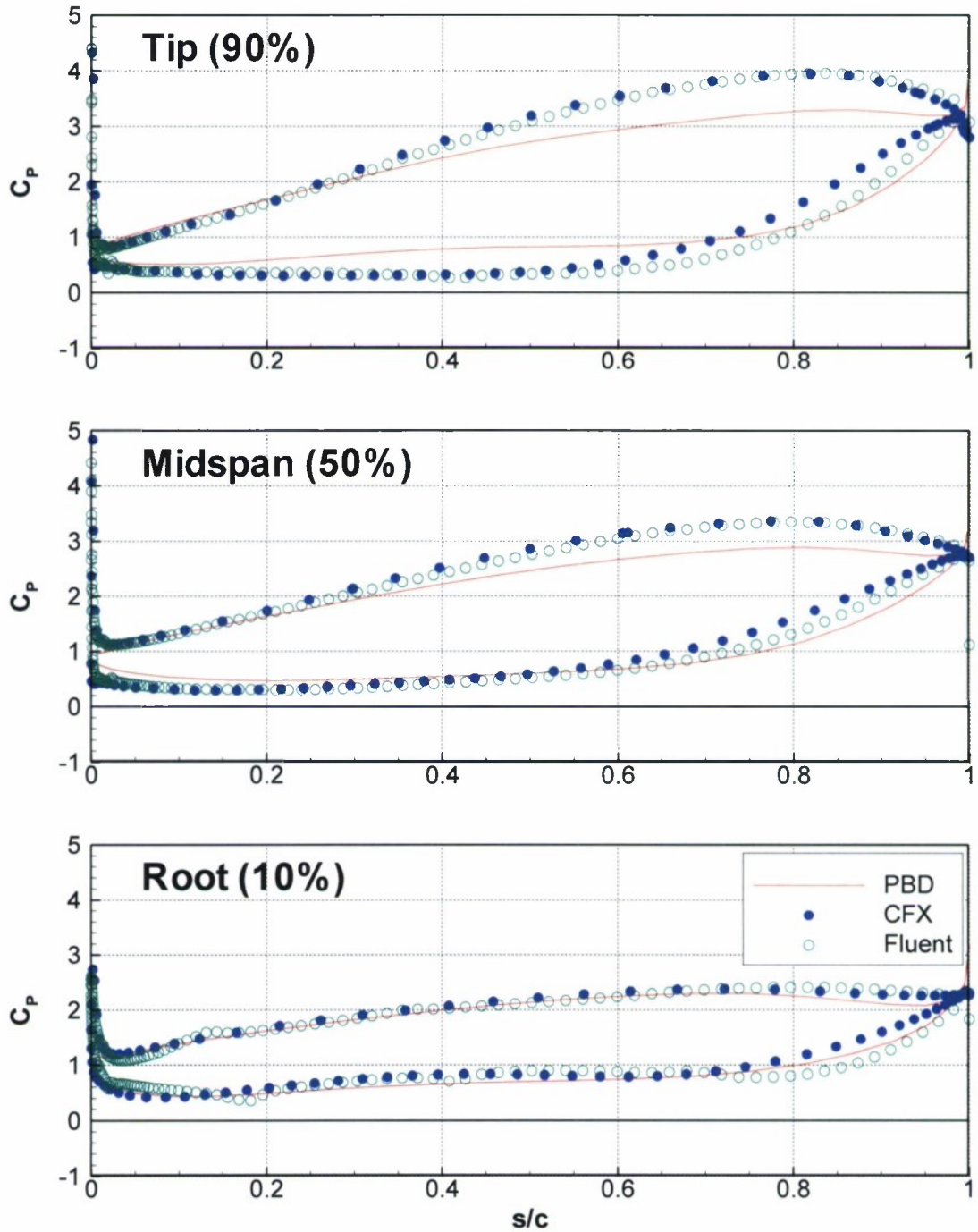

Figure 10. Rotor sectional pressure distributions.

C_P=0 represents vapor pressure.

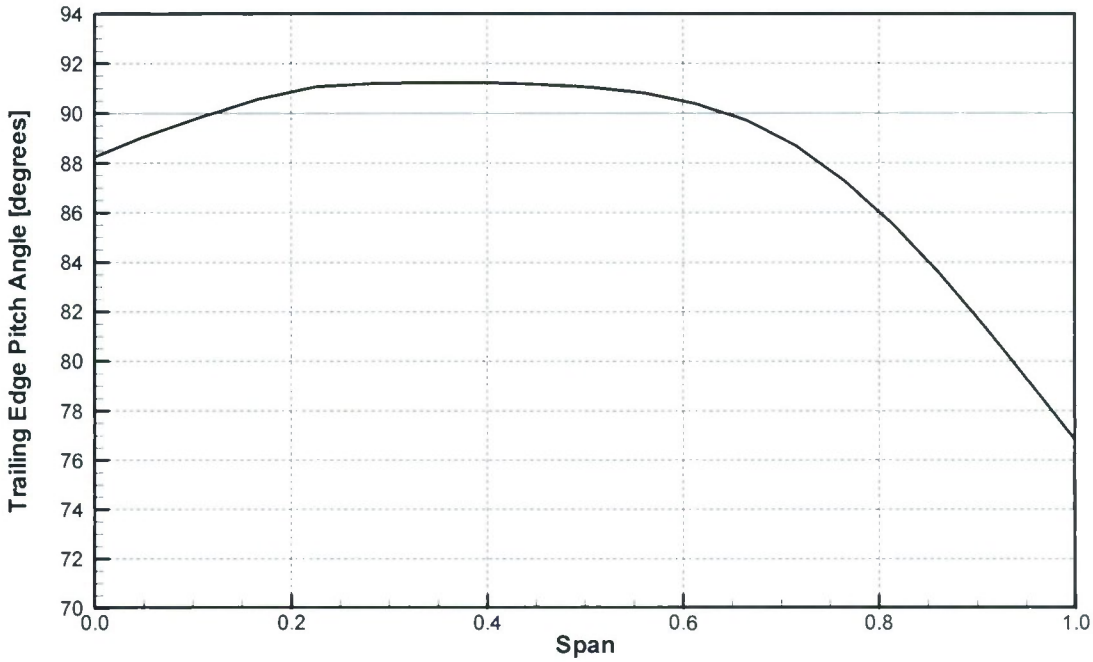

Figure 11. Stator trailing edge pitch angle.

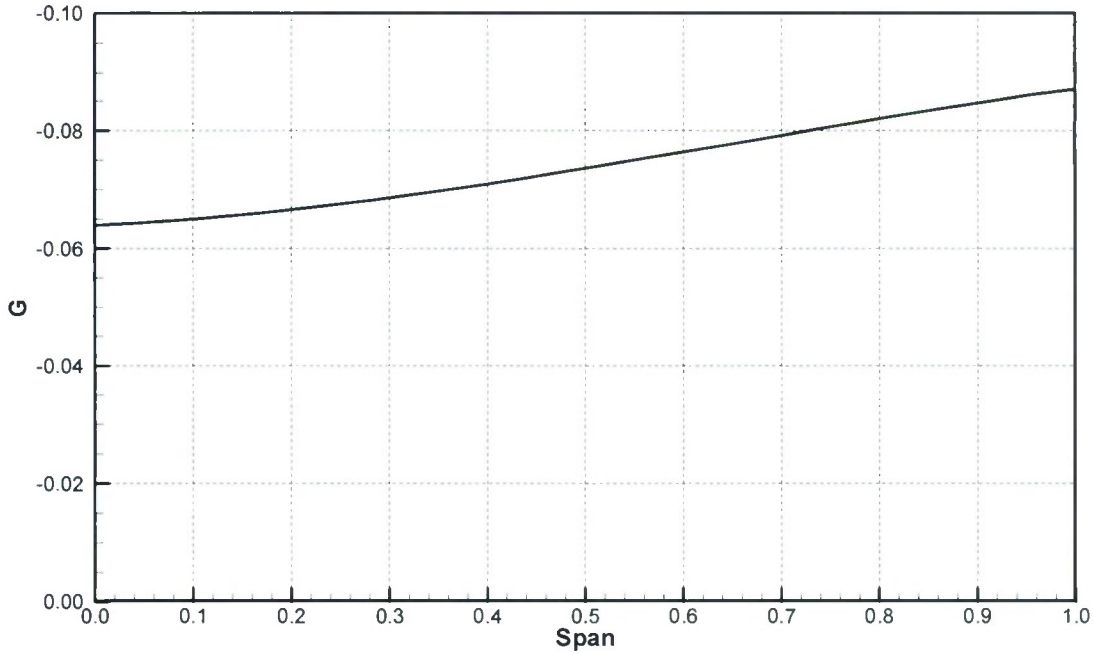

Figure 12. Stator spanwise circulation distribution.

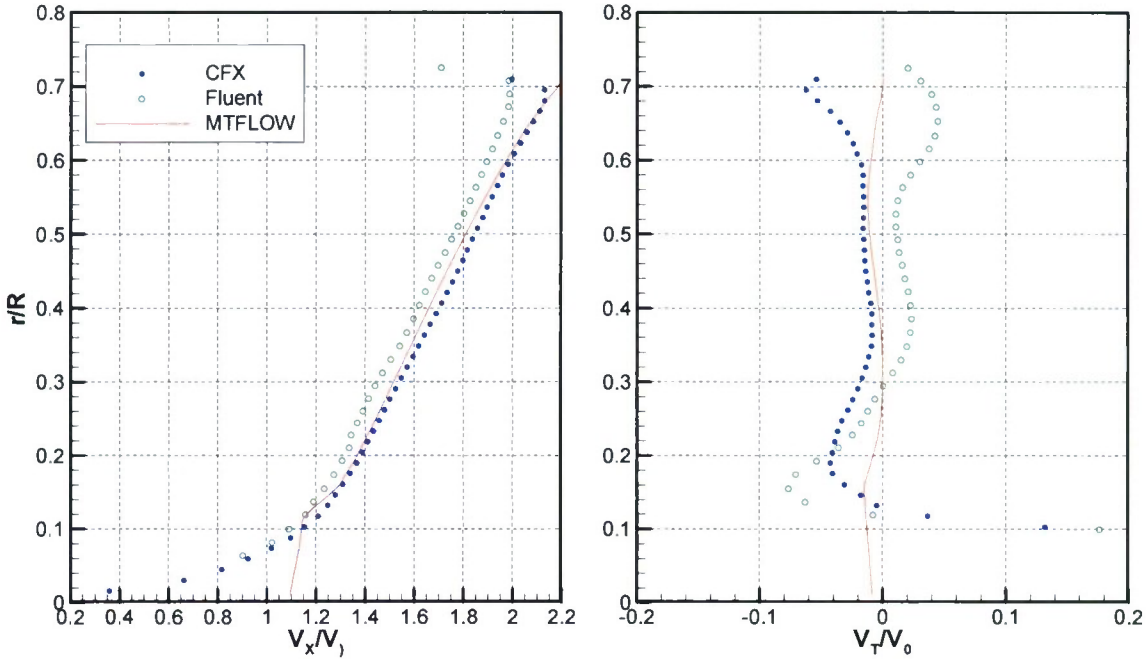

Figure 13. Velocity at a plane downstream of stator.

x/R = 2.12

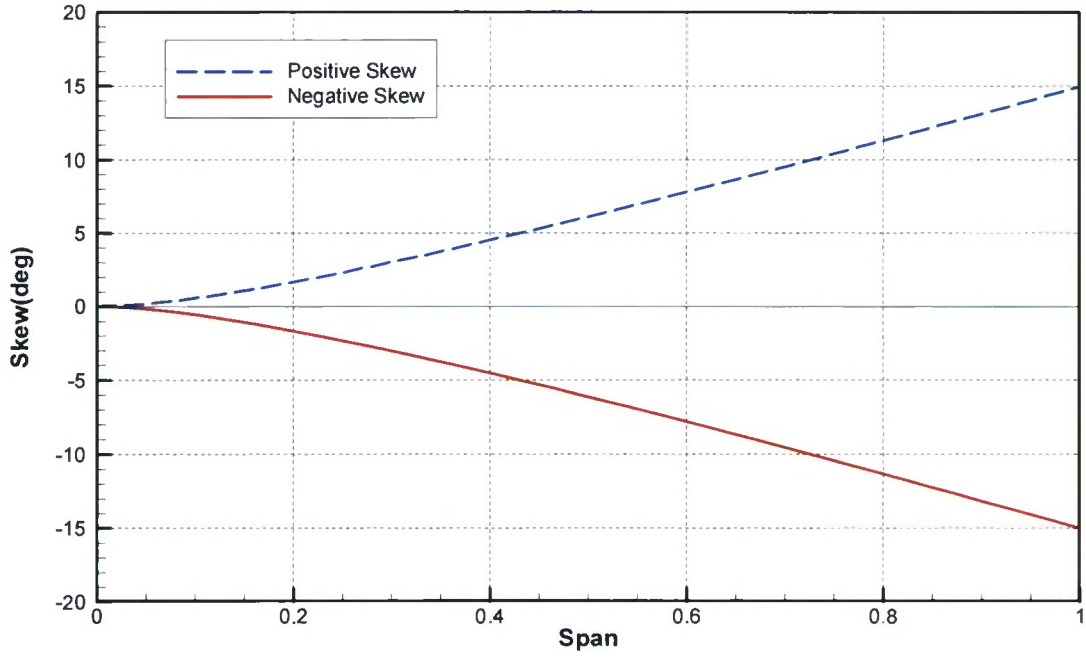

Figure 14. Stator skew distributions for pressure comparison.

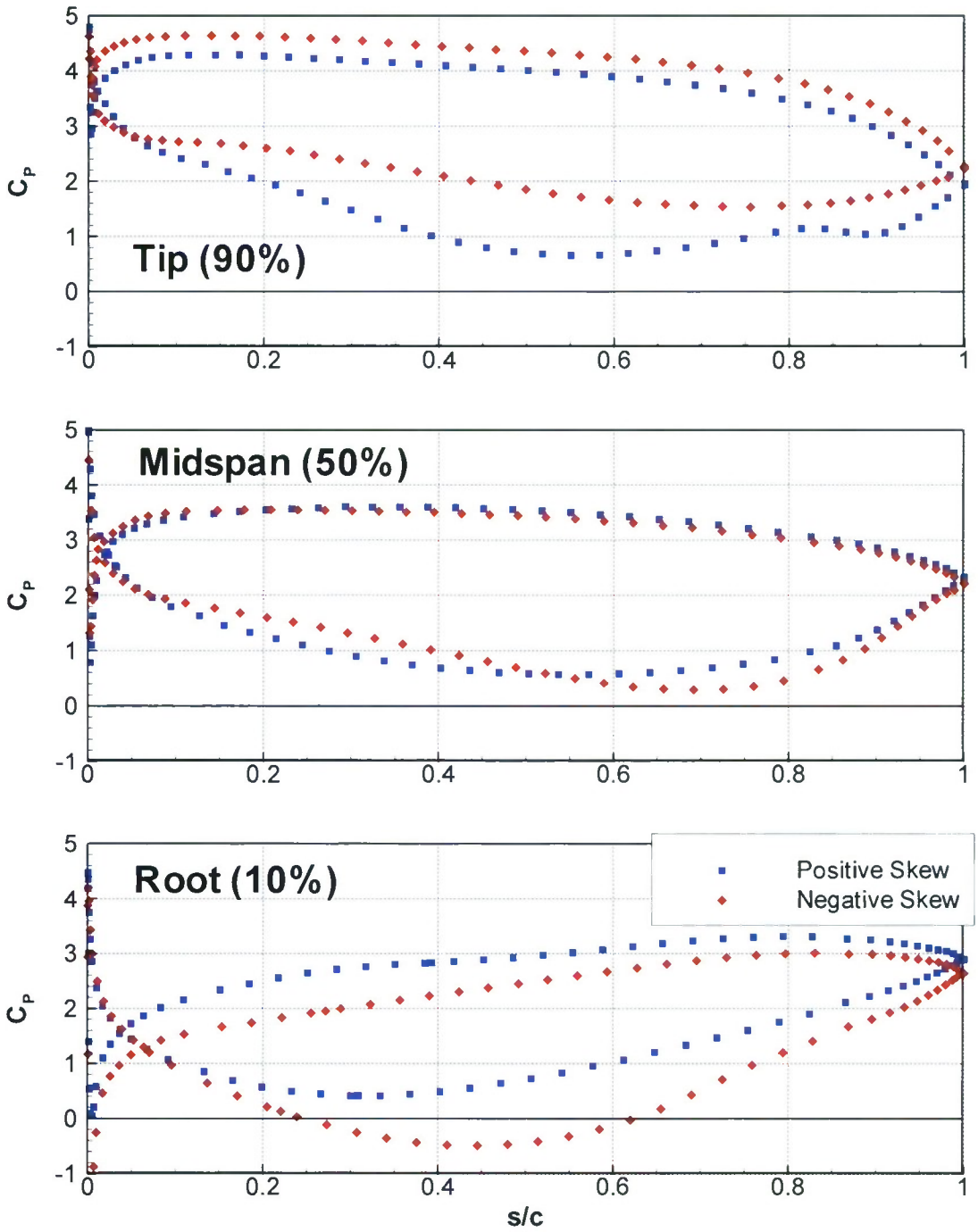

Figure 15. Stator chordwise pressure distributions, +15 and -15 degrees of skew (CFX).

For skew distribution details, see Figure 14.

C_P=0 represents vapor pressure.

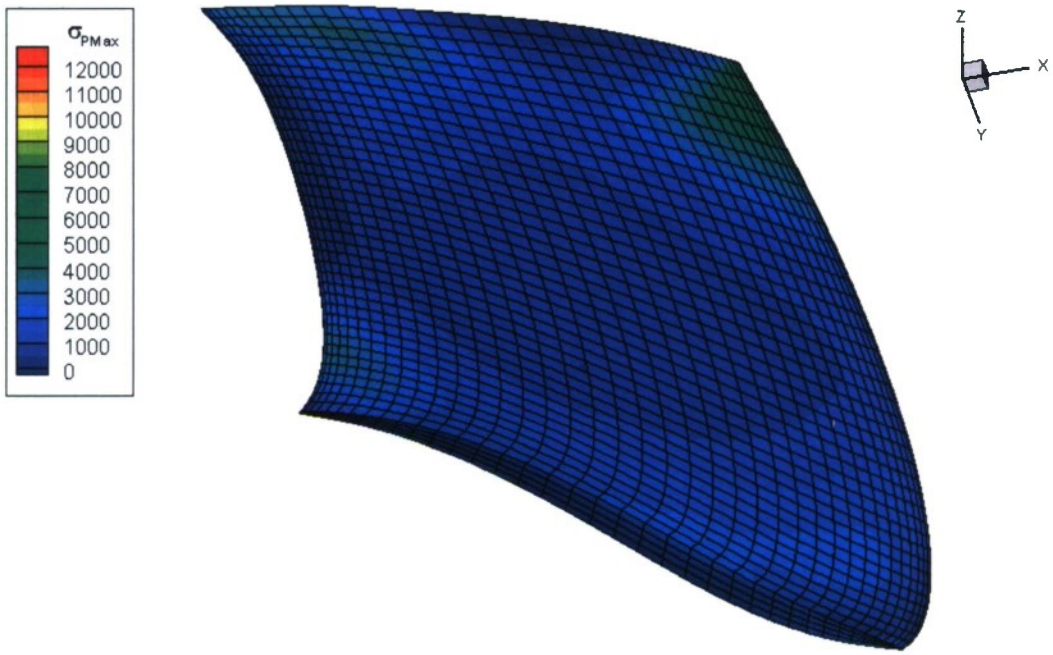

Figure 16. Stator pressure side maximum principal stress distribution in psi. Assumes 67 inch (1700 mm) diameter pump, nickel-aluminum-bronze.

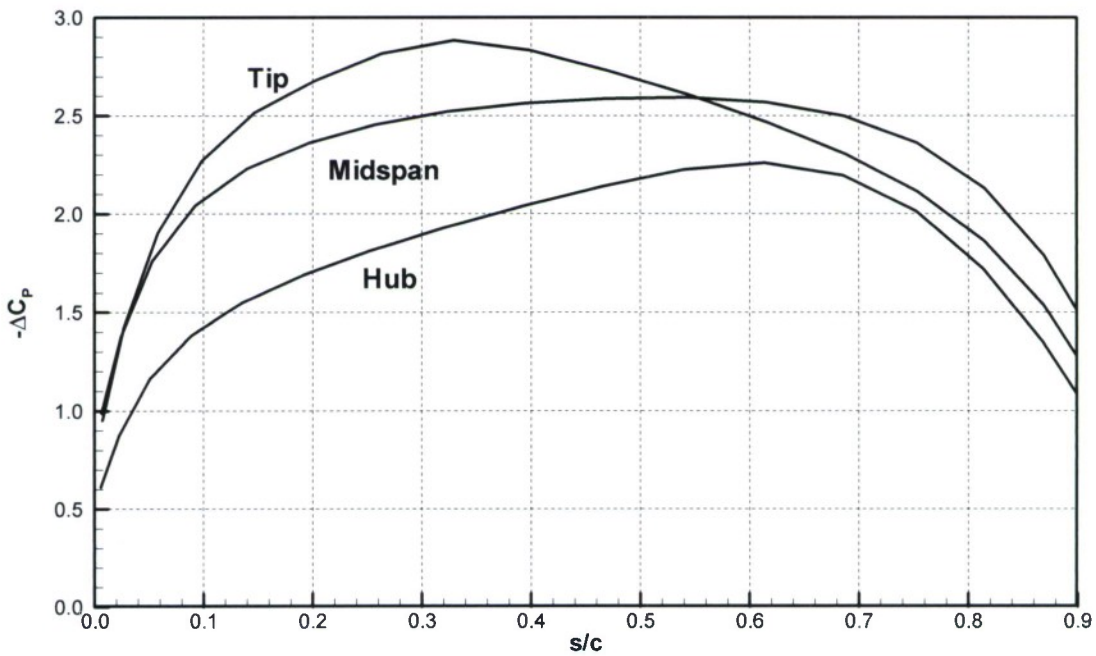

Figure 17. Stator chordwise loading distribution (PBD-14).

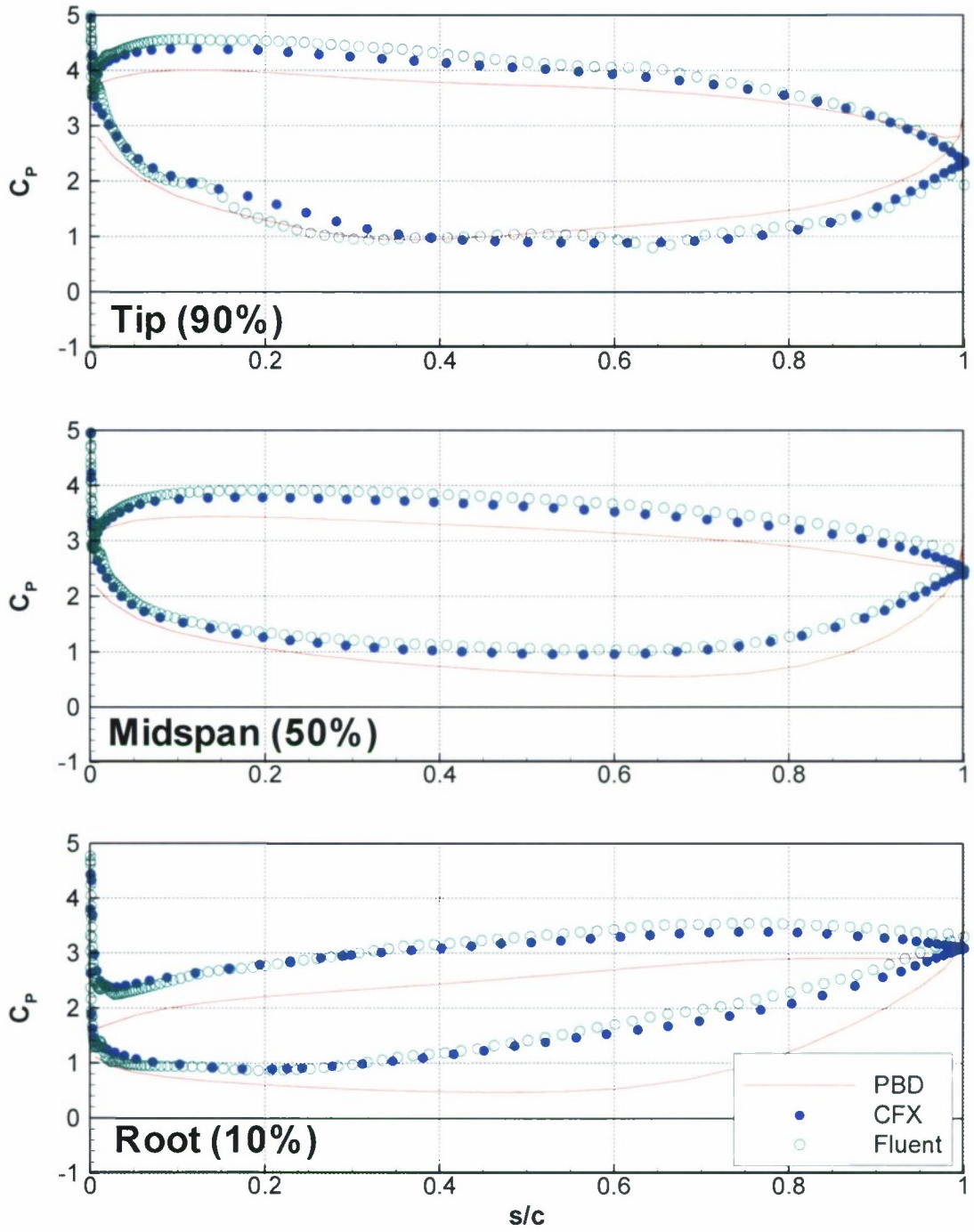

Figure 18. Stator sectional pressure distributions.

C_P=0 represents vapor pressure.

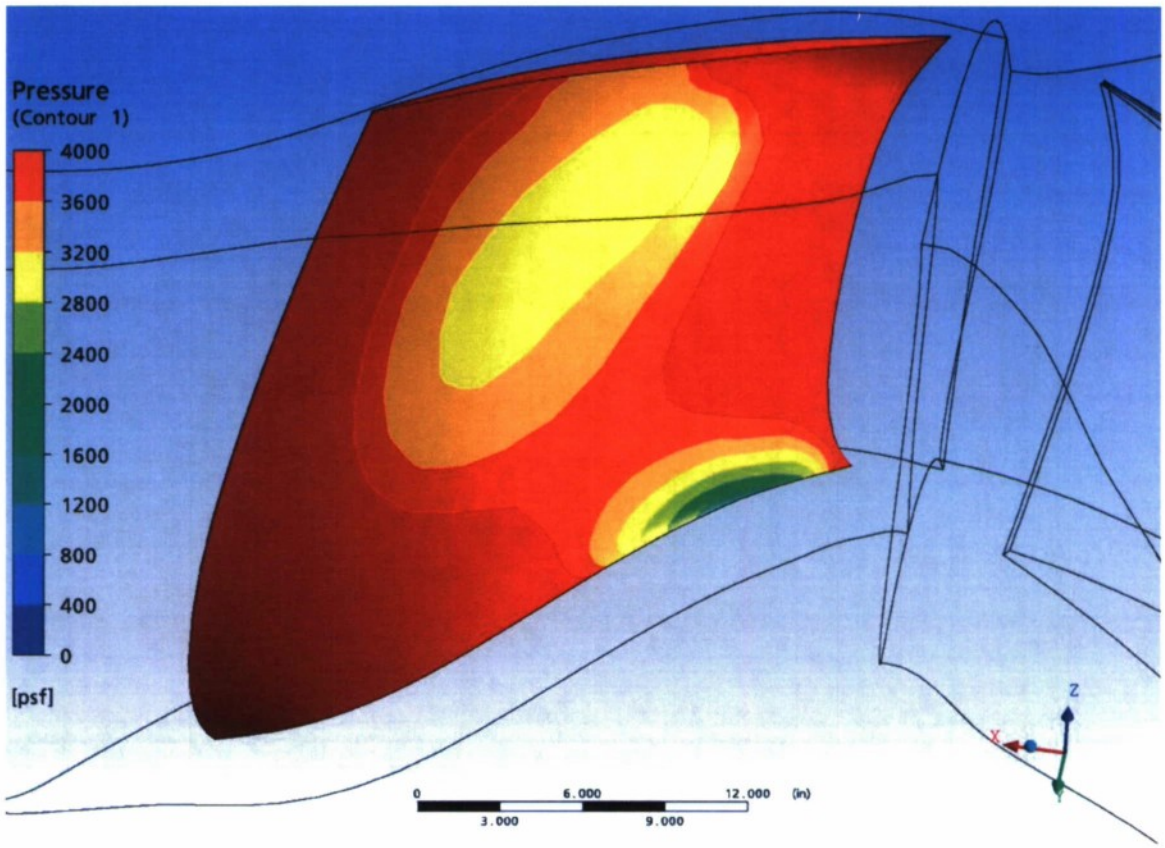

Figure 19. Stator suction side pressure distribution from CFX.

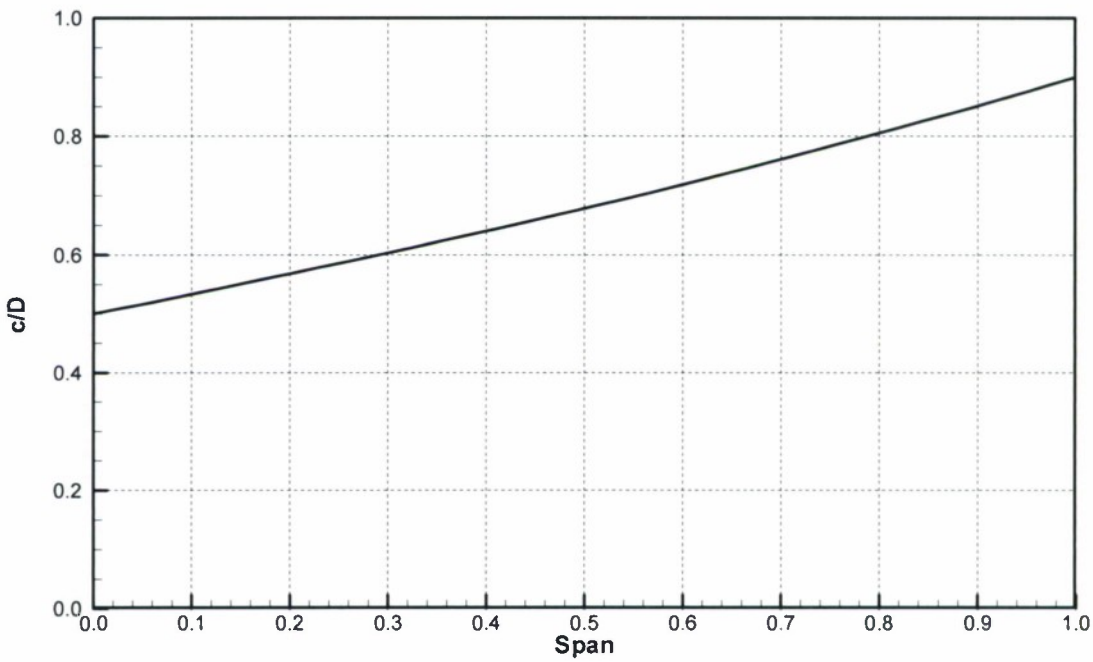

Figure 20. Rotor spanwise chord distribution.

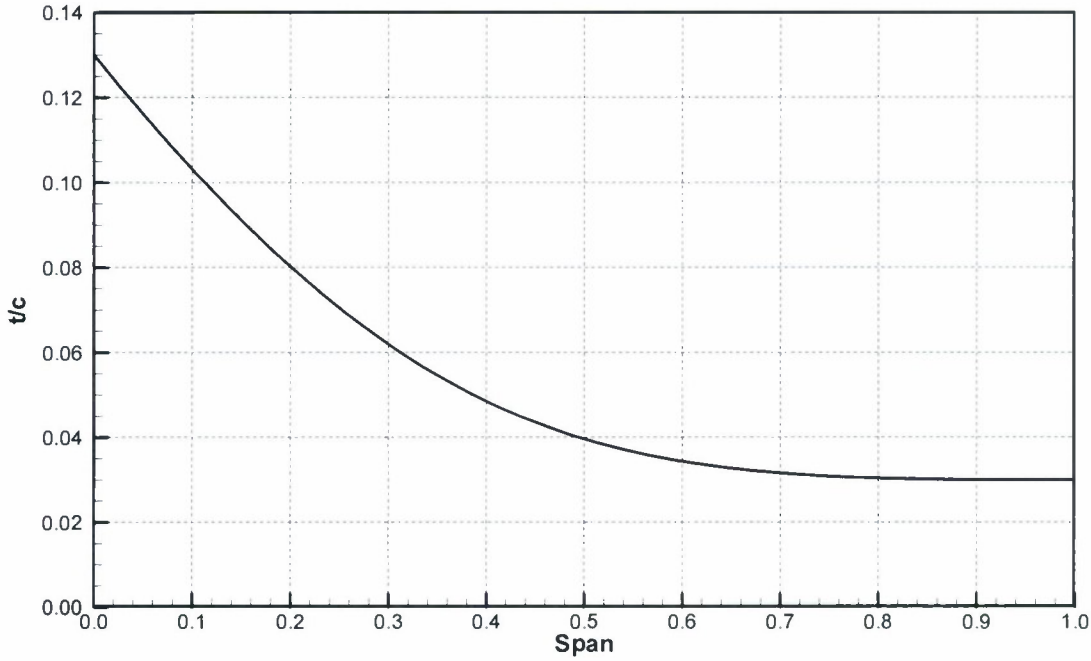

Figure 21. Rotor spanwise thickness distribution.

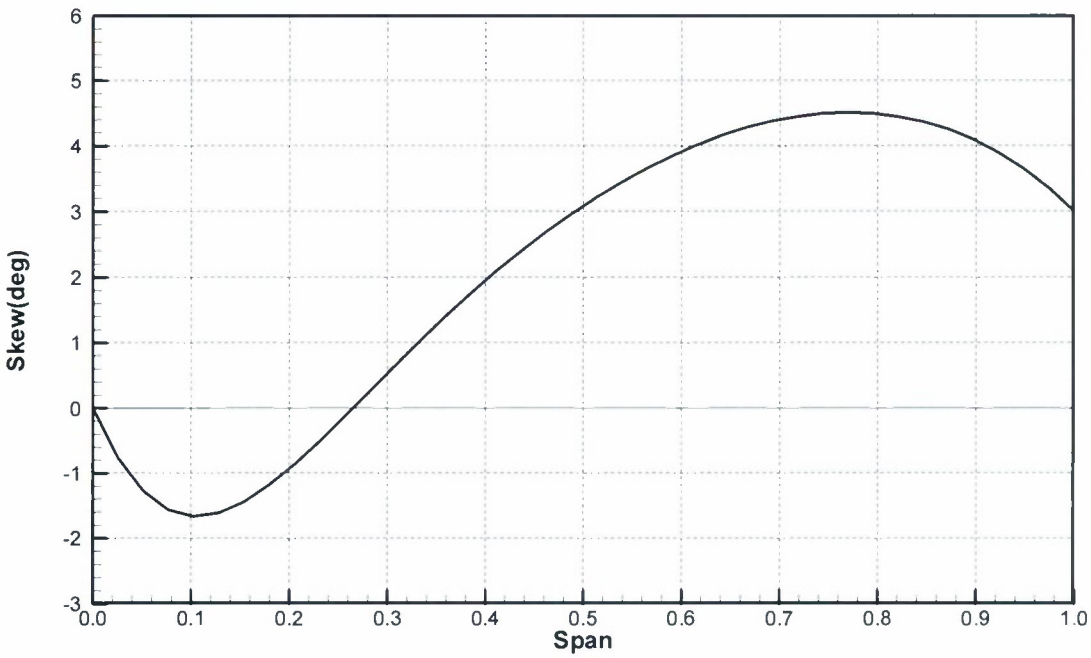

Figure 22. Rotor spanwise skew distribution.

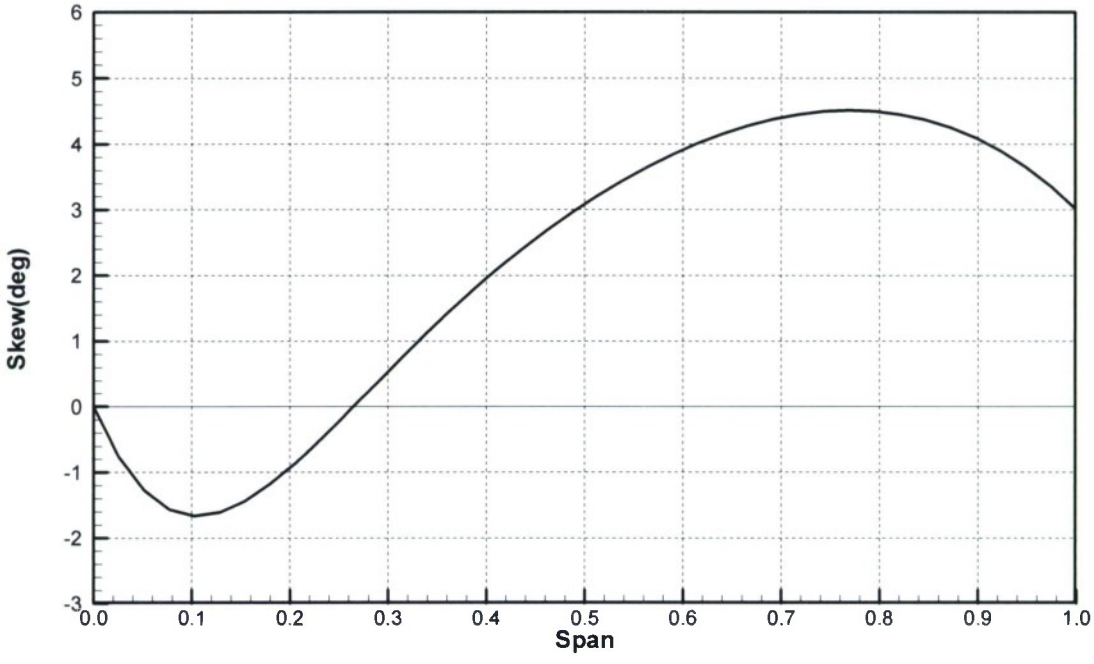

Figure 23. Rotor spanwise rake distribution.

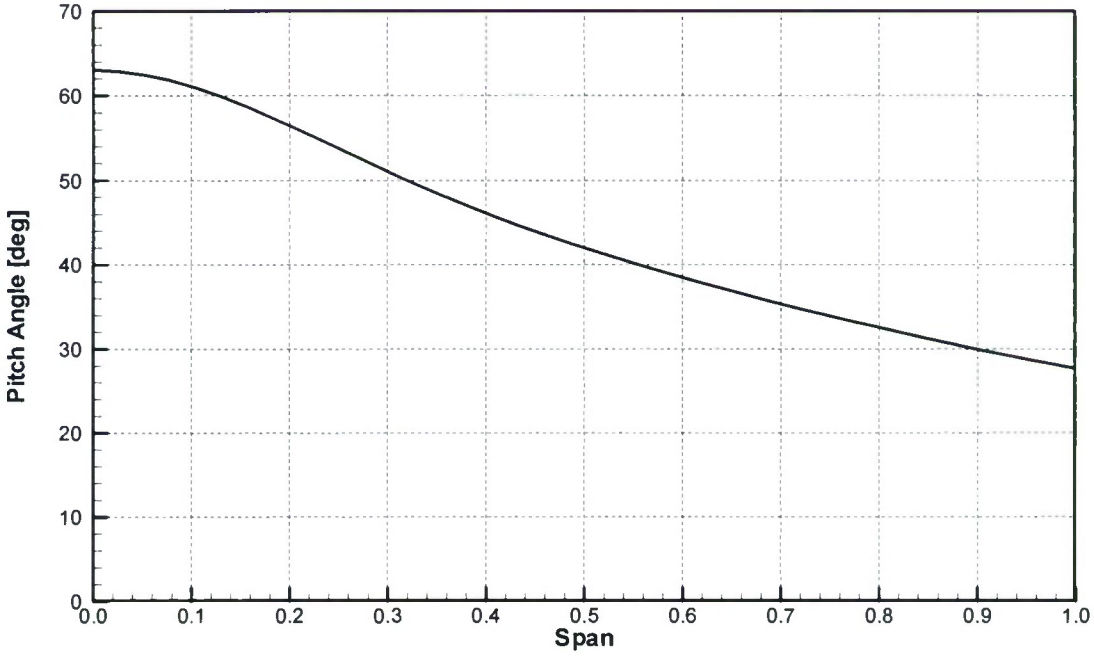

Figure 24. Rotor spanwise pitch distribution.

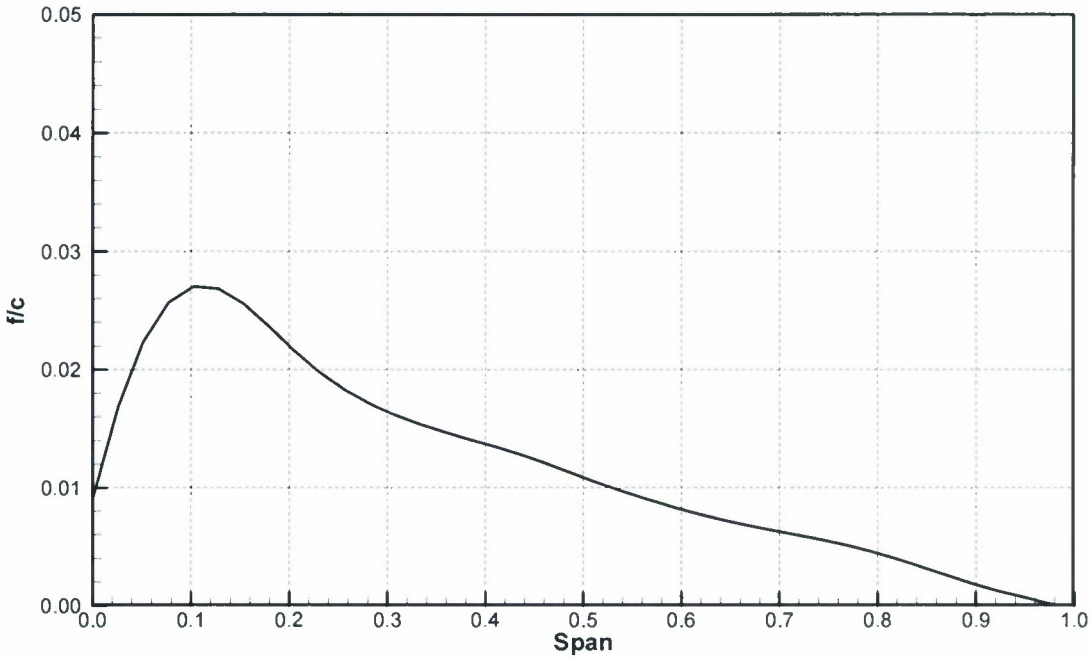

Figure 25. Rotor spanwise camber distribution.

(This is the distribution at midchord; f/c is set to zero at 0.75c.)

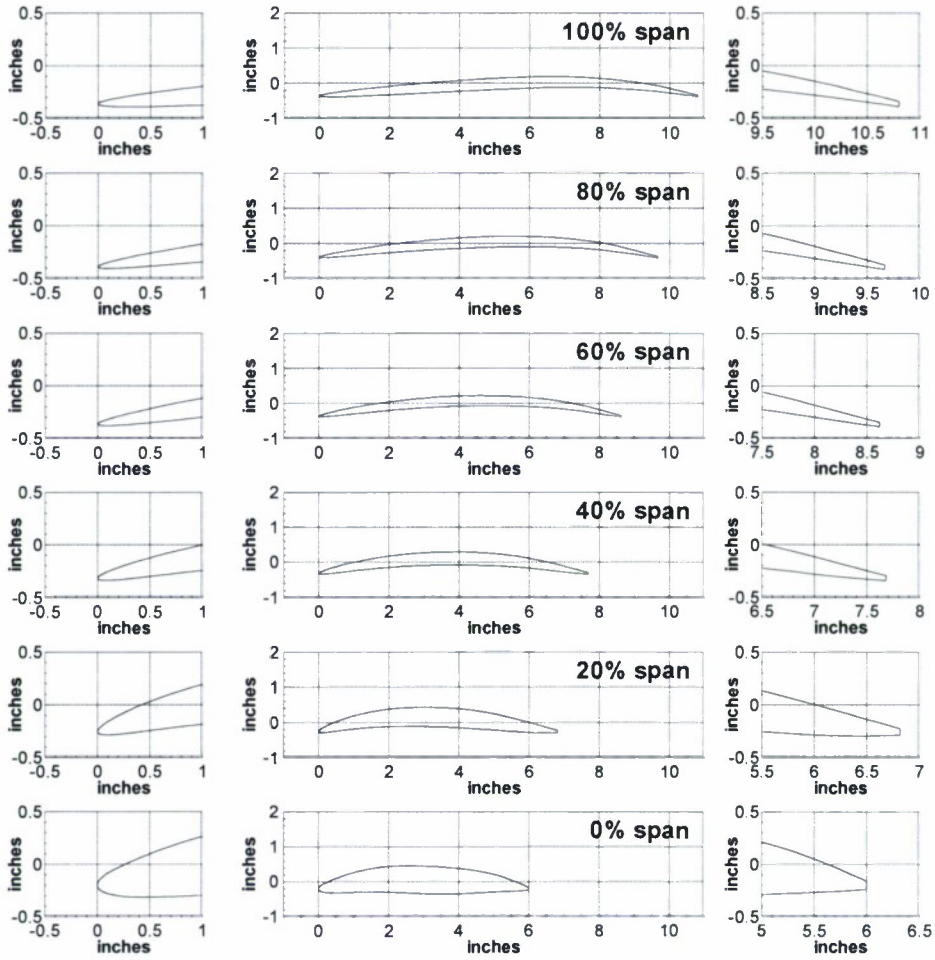

Figure 26. Rotor section shapes.

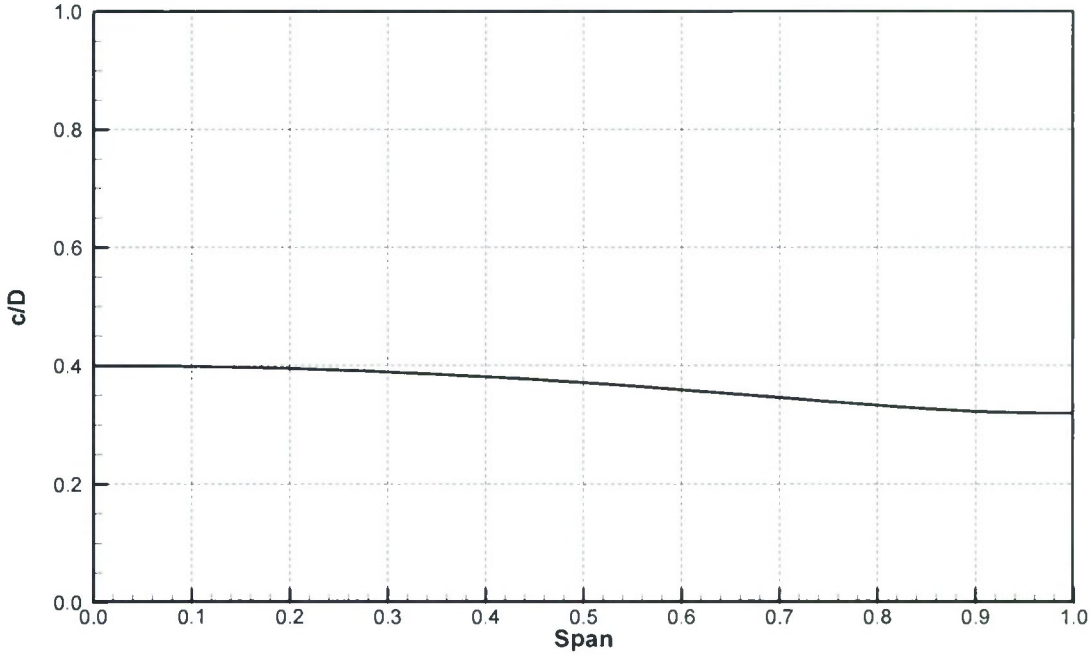

Figure 27. Stator spanwise chord distribution.

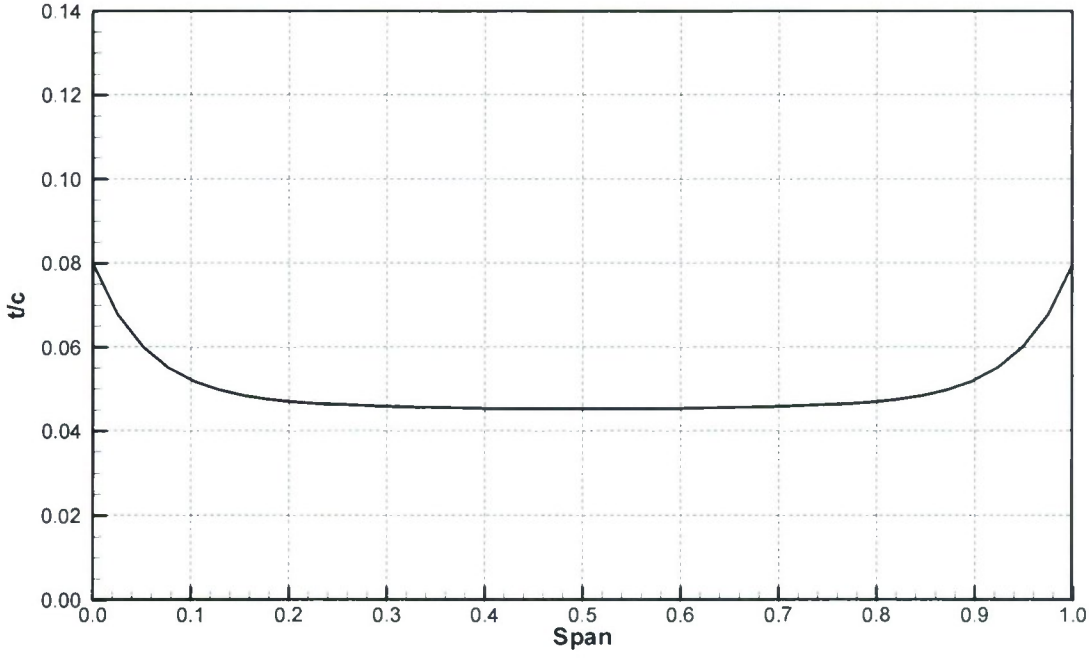

Figure 28. Stator spanwise thickness distribution.

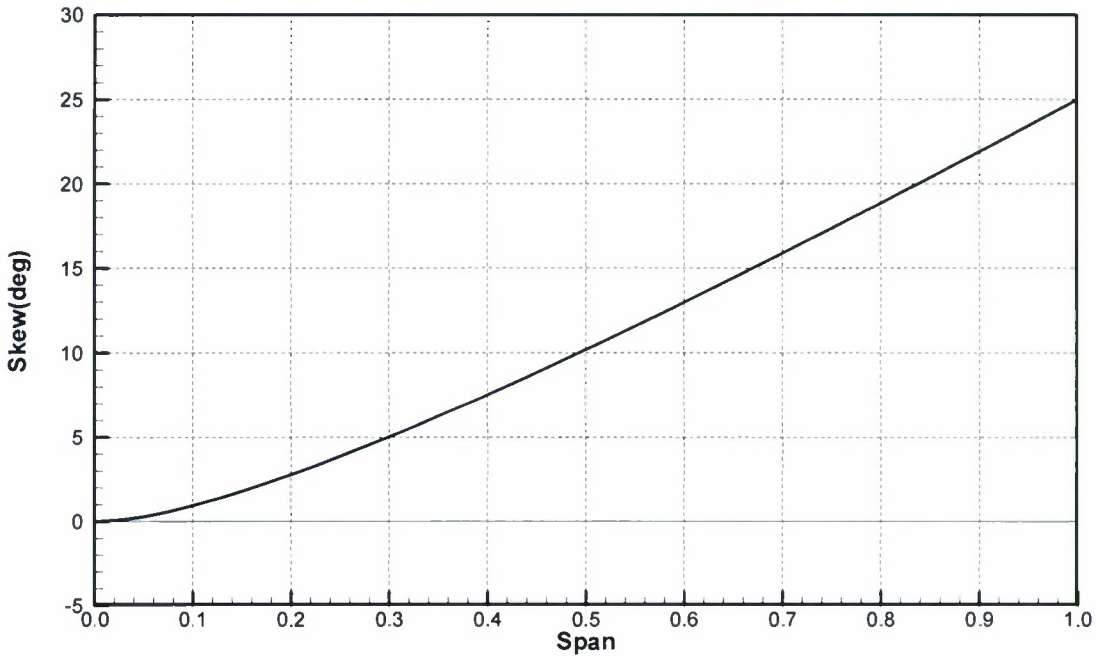

Figure 29. Stator spanwise skew distribution.

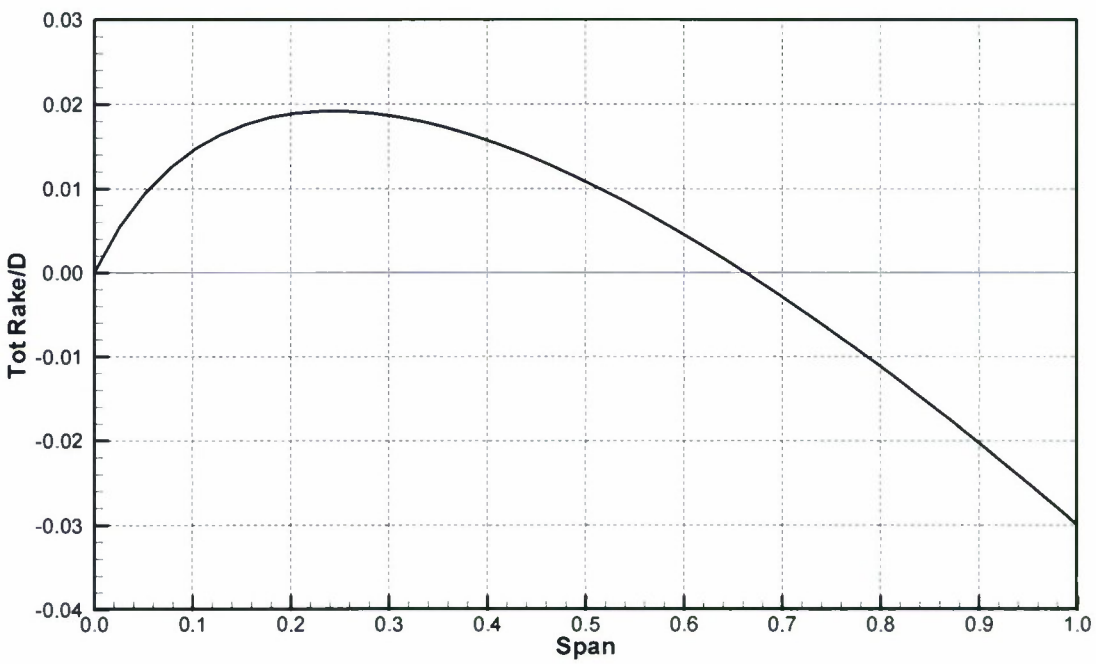

Figure 30. Stator spanwise rake distribution.

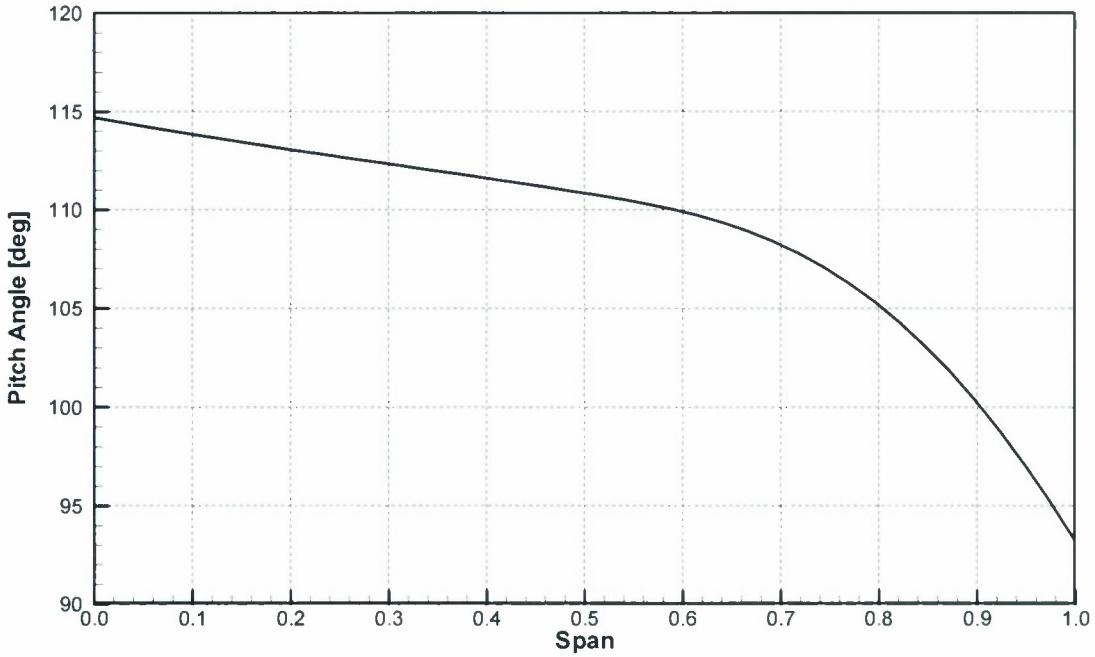

Figure 31. Stator spanwise pitch distribution.

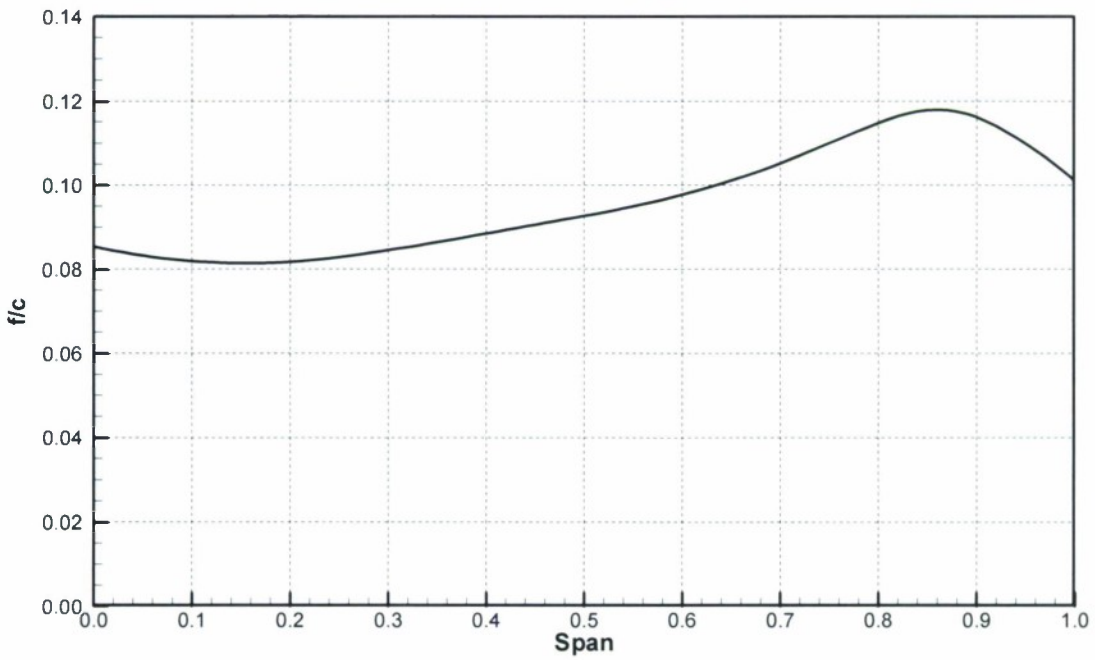

Figure 32. Stator spanwise camber distribution.

(This is the distribution at the leading edge; f/c is set to zero at midchord.)

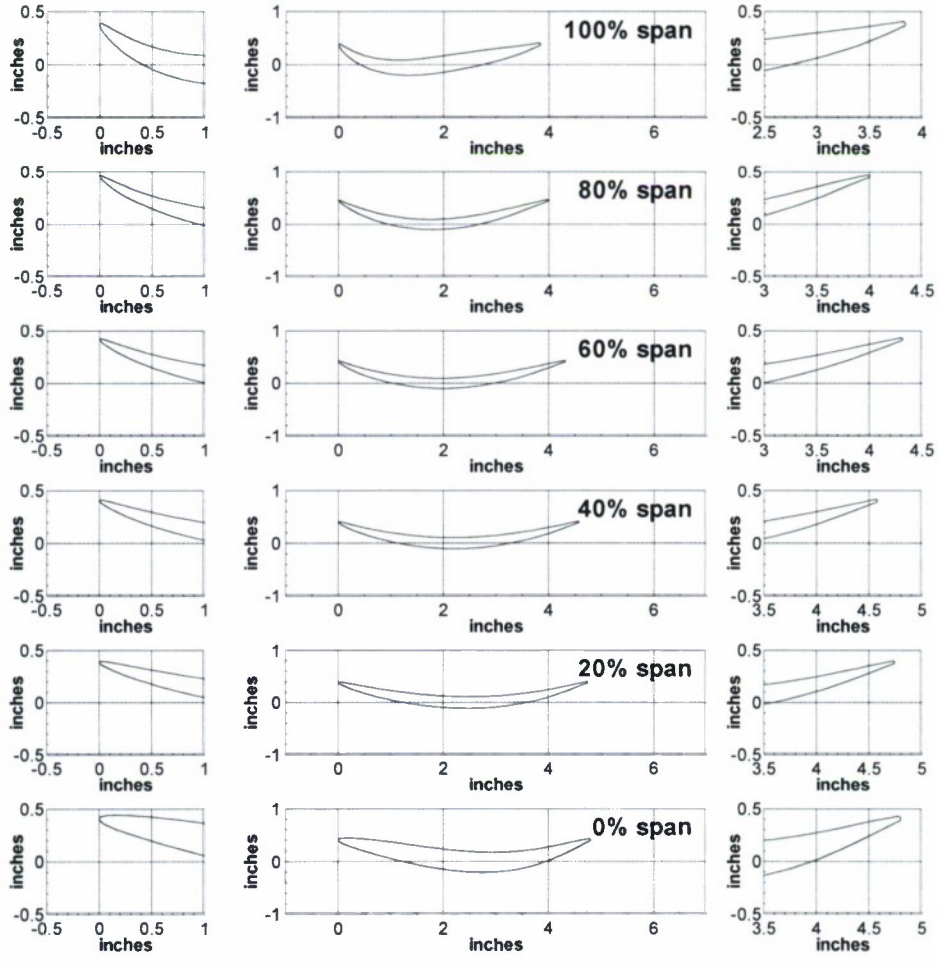

Figure 33. Stator section shapes.

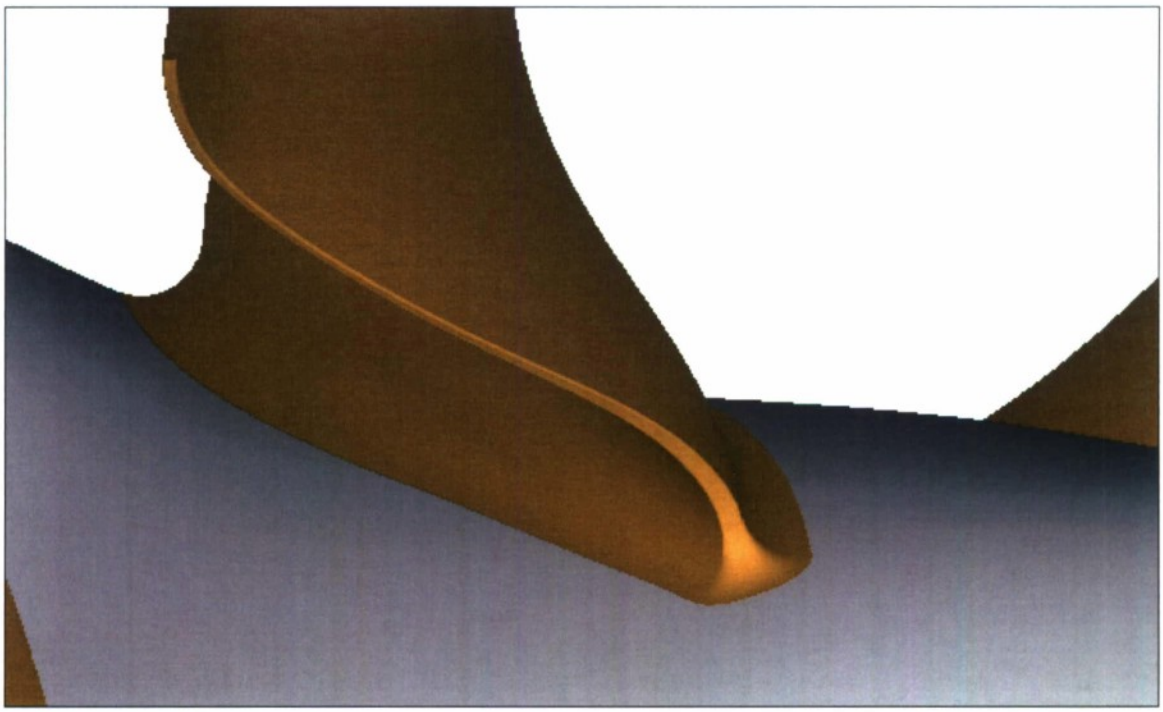

Figure 34. Rotor trailing edge.

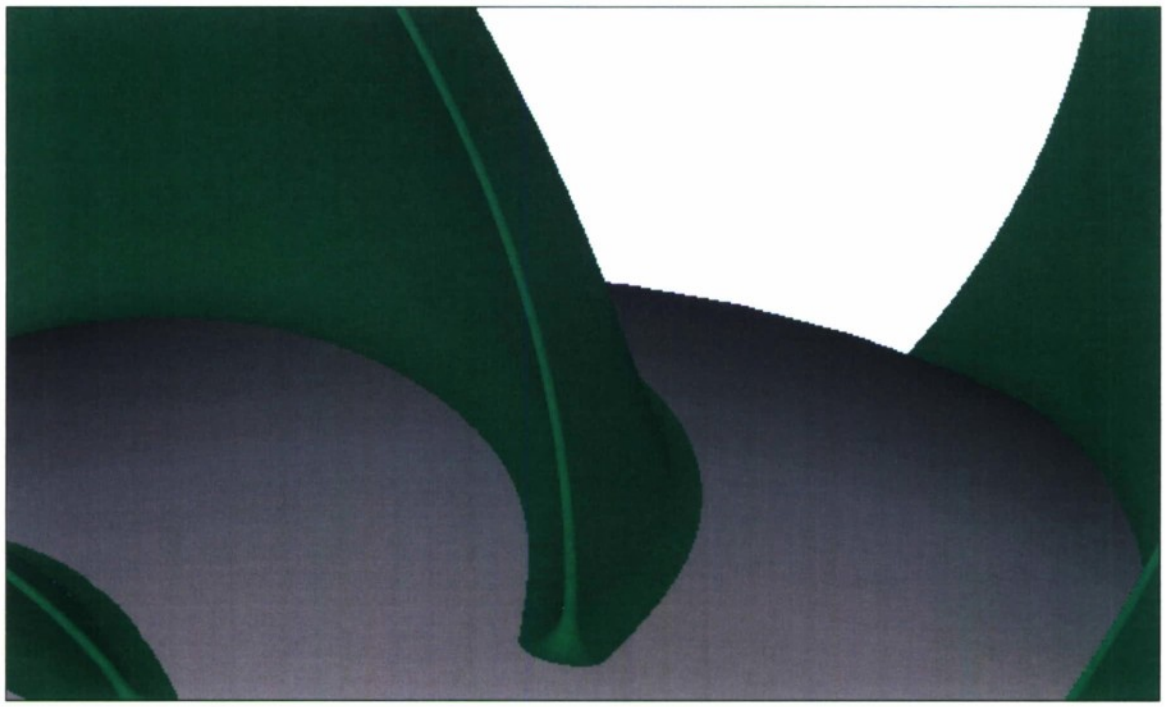

Figure 35. Stator trailing edge.

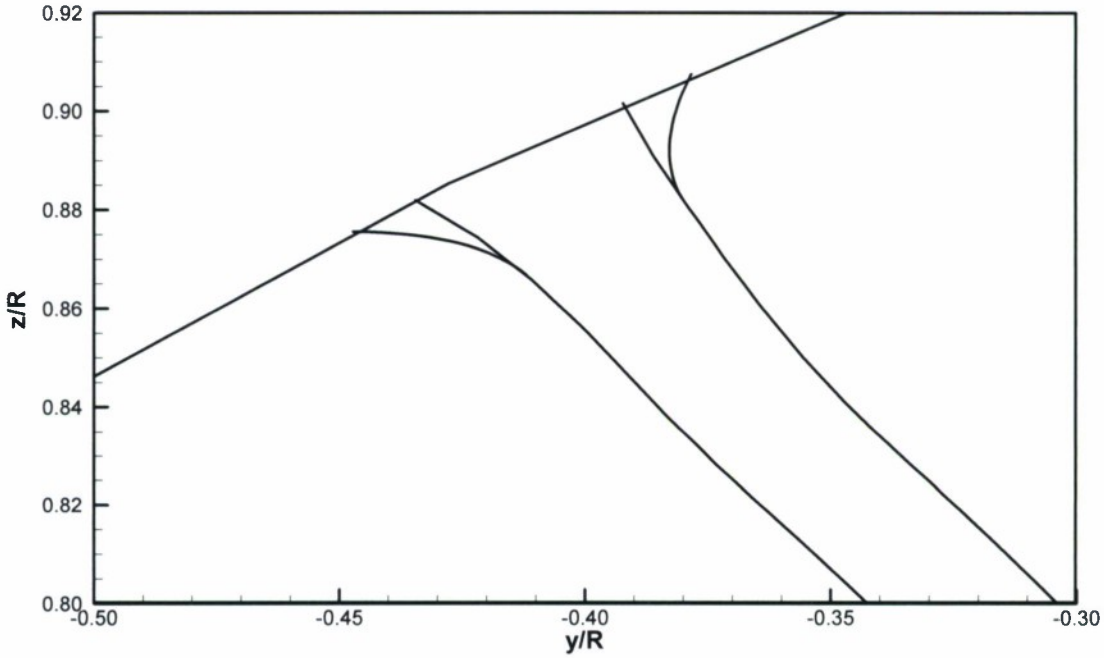

Figure 36. Stator tip fillet, section at x/R=1.35.

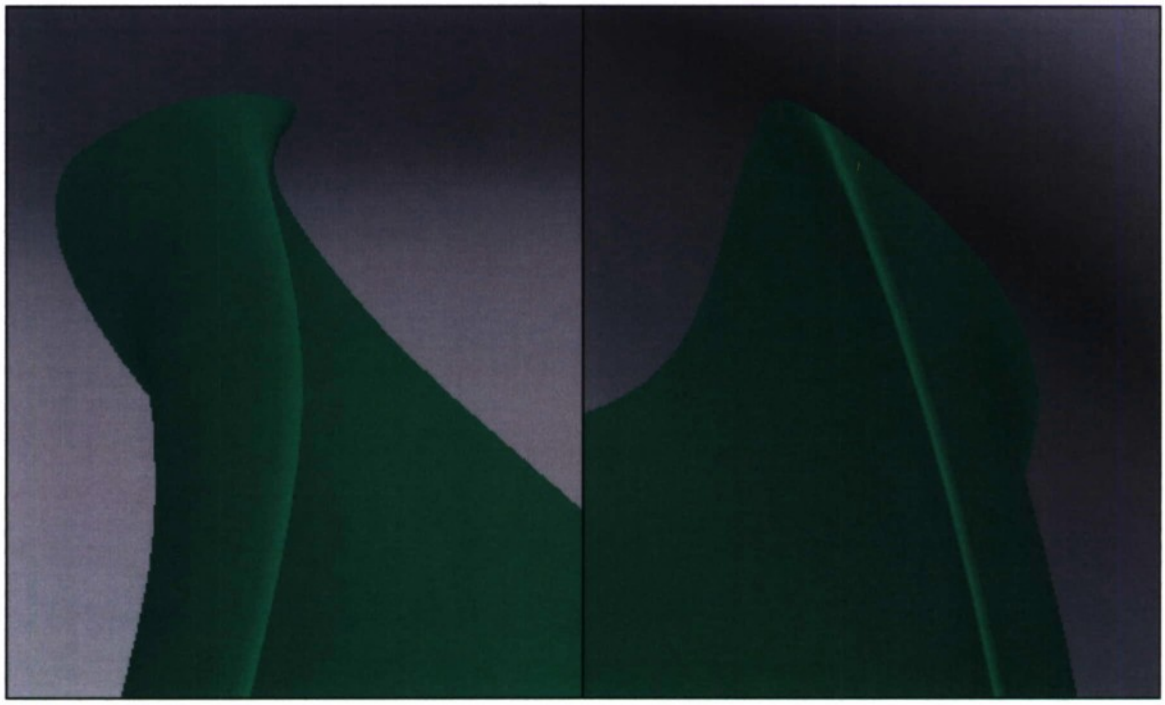

Figure 37. Stator tip fillet.

Leading edge, left, and trailing edge, right.

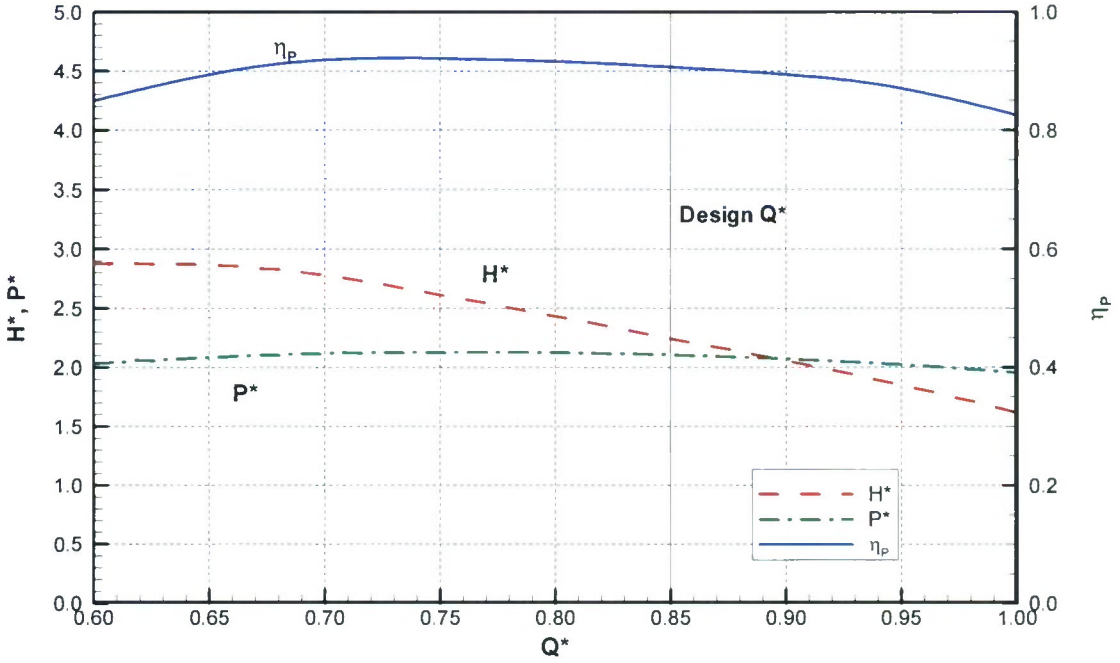

Figure 38. Performance of a 12 inch (304.8 mm) pump.

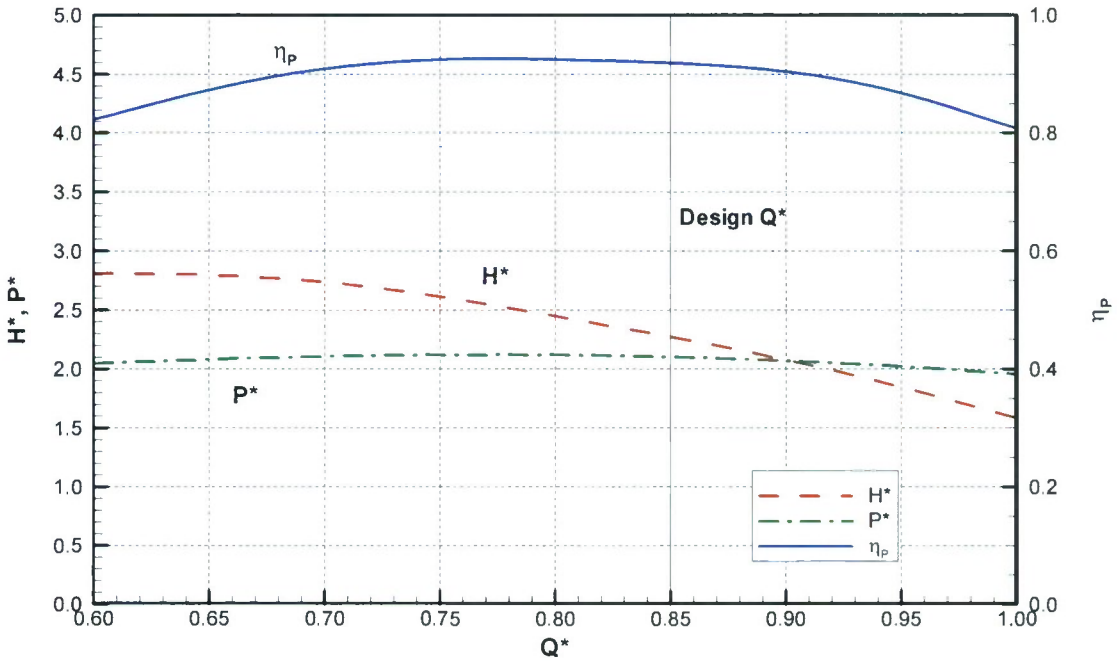

Figure 39. Performance of a 70 inch (1778 mm) pump.

APPENDIX A: GEOMETRY TABLES

HUB AND CASING GEOMETRY

The hub and casing geometry is normalized by the inlet radius. Table A-1 lists the hub and casing geometry.

Table A-1. Hub and casing geometry.

x/R	Hub r/R	Casing r/R
-1.000000	0.300000	1.000000
-0.900000	0.300000	1.000000
-0.800000	0.300000	1.000000
-0.700000	0.300000	1.000000
-0.600000	0.300000	1.000000
-0.500000	0.300000	1.000000
-0.400000	0.300000	1.000000
-0.300000	0.300000	1.000000
-0.200000	0.300000	1.000000
-0.100000	0.300000	1.000000
0.000000	0.300000	1.000000
0.100000	0.301044	1.000000
0.200000	0.306413	1.000000
0.300000	0.317749	1.000000
0.400000	0.335955	1.000000
0.500000	0.361397	1.000000
0.600000	0.391523	1.000000
0.700000	0.423044	1.000000
0.800000	0.453446	1.000000
0.900000	0.480780	1.000000
1.000000	0.503516	1.000000

Table A-1 (continued). Hub and casing geometry.

x/R	Hub r/R	Casing r/R
1.100000	0.519828	1.000000
1.200000	0.523967	0.999921
1.300000	0.512022	0.992678
1.400000	0.484104	0.971635
1.500000	0.442100	0.944660
1.600000	0.388240	0.912435
1.700000	0.324539	0.872455
1.800000	0.252661	0.825882
1.900000	0.173940	0.780784
2.000000	0.089438	0.744816
2.100000	0.000000	0.720391
2.200000	0.000000	0.707317
2.300000	0.000000	0.701536
2.400000	0.000000	0.700031
2.500000	0.000000	0.700000

ROTOR GEOMETRY

Table A-2 lists the rotor spanwise geometric characteristics. The rotor reference line is defined by two points. One is located at x/R=0.80 relative to the upstream end of the rotor hub and r/R=0.30. The second point is located at x/R=0.75 and r/R=1.20. Tables A-3 through A-8 contain selected section shapes. The spanwise data and blade sections are defined on the section generation curves, which are uniformly spaced between the hub and casing, and shown earlier in Figure 3.

Table A-2. Rotor spanwise geometry.

span	c/D	t/c	t/D	Pitch (deg)	Skew (deg)	Rake/D
0.00	0.5000	0.1300	0.0650	63.09	0.000	0.0000
0.05	0.5167	0.1161	0.0600	62.51	-1.254	-0.0059
0.10	0.5337	0.1031	0.0550	61.10	-1.659	-0.0111
0.15	0.5508	0.0911	0.0502	59.01	-1.471	-0.0158
0.20	0.5681	0.0802	0.0456	56.48	-0.932	-0.0201
0.25	0.5857	0.0705	0.0413	53.76	-0.223	-0.0239
0.30	0.6035	0.0619	0.0374	51.05	0.537	-0.0273
0.35	0.6216	0.0546	0.0340	48.47	1.277	-0.0304
0.40	0.6401	0.0485	0.0311	46.10	1.955	-0.0331
0.45	0.6589	0.0436	0.0287	43.95	2.559	-0.0356
0.50	0.6782	0.0396	0.0269	42.00	3.088	-0.0377
0.55	0.6980	0.0366	0.0256	40.19	3.542	-0.0395
0.60	0.7184	0.0344	0.0247	38.49	3.915	-0.0409
0.65	0.7395	0.0327	0.0242	36.89	4.205	-0.0420
0.70	0.7612	0.0316	0.0241	35.37	4.403	-0.0424
0.75	0.7833	0.0309	0.0242	33.92	4.502	-0.0419
0.80	0.8056	0.0304	0.0245	32.54	4.491	-0.0401
0.85	0.8281	0.0302	0.0250	31.23	4.356	-0.0369
0.90	0.8513	0.0300	0.0256	29.98	4.080	-0.0322
0.95	0.8753	0.0300	0.0263	28.79	3.638	-0.0264
1.00	0.9000	0.0300	0.0270	27.67	3.000	-0.0200

Table A-3. Rotor section shape, 0% span.

s/c	h/c Back	h/c Face
0.0000	-0.03345	-0.03345
0.0043	-0.02406	-0.04061
0.0170	-0.01403	-0.04653
0.0381	-0.00290	-0.05069
0.0670	0.00992	-0.05240
0.1033	0.02404	-0.05196
0.1464	0.03836	-0.05030
0.1956	0.05150	-0.04863
0.2500	0.06226	-0.04790
0.3087	0.07003	-0.04843
0.3706	0.07455	-0.05017
0.4347	0.07572	-0.05293
0.5000	0.07401	-0.05599
0.5653	0.07061	-0.05795
0.6294	0.06615	-0.05785
0.6913	0.06041	-0.05581
0.7500	0.05268	-0.05270
0.8044	0.04245	-0.04956
0.8536	0.02990	-0.04703
0.8967	0.01596	-0.04522
0.9330	0.00206	-0.04391
0.9619	-0.01027	-0.04250
0.9830	-0.01951	-0.04116
0.9957	-0.02512	-0.04035
1.0000	-0.02822	-0.03833

Table A-4. Rotor section shape, 20% span.

s/c	h/c Back	h/c Face
0.0000	-0.03722	-0.03722
0.0043	-0.03065	-0.04086
0.0170	-0.02161	-0.04166
0.0381	-0.01050	-0.03998
0.0670	0.00202	-0.03643
0.1033	0.01508	-0.03180
0.1464	0.02784	-0.02686
0.1956	0.03947	-0.02231
0.2500	0.04924	-0.01872
0.3087	0.05662	-0.01647
0.3706	0.06126	-0.01568
0.4347	0.06306	-0.01630
0.5000	0.06210	-0.01810
0.5653	0.05850	-0.02081
0.6294	0.05227	-0.02425
0.6913	0.04350	-0.02826
0.7500	0.03255	-0.03260
0.8044	0.02024	-0.03677
0.8536	0.00774	-0.04010
0.8967	-0.00390	-0.04219
0.9330	-0.01403	-0.04309
0.9619	-0.02217	-0.04287
0.9830	-0.02808	-0.04231
0.9957	-0.03160	-0.04198
1.0000	-0.03398	-0.04023

Table A-5. Rotor section shape, 40% span.

s/c	h/c Back	h/c Face
0.0000	-0.04158	-0.04158
0.0043	-0.03752	-0.04370
0.0170	-0.03174	-0.04388
0.0381	-0.02442	-0.04226
0.0670	-0.01587	-0.03914
0.1033	-0.00655	-0.03491
0.1464	0.00304	-0.03006
0.1956	0.01233	-0.02505
0.2500	0.02078	-0.02035
0.3087	0.02790	-0.01633
0.3706	0.03329	-0.01327
0.4347	0.03670	-0.01133
0.5000	0.03798	-0.01055
0.5653	0.03702	-0.01098
0.6294	0.03363	-0.01268
0.6913	0.02780	-0.01566
0.7500	0.01974	-0.01977
0.8044	0.00993	-0.02473
0.8536	-0.00083	-0.03003
0.8967	-0.01149	-0.03501
0.9330	-0.02104	-0.03910
0.9619	-0.02875	-0.04179
0.9830	-0.03427	-0.04345
0.9957	-0.03750	-0.04445
1.0000	-0.03967	-0.04317

Table A-6. Rotor section shape, 60% span.

s/c	h/c Back	h/c Face
0.0000	-0.04248	-0.04248
0.0043	-0.03957	-0.04394
0.0170	-0.03532	-0.04392
0.0381	-0.02984	-0.04248
0.0670	-0.02330	-0.03978
0.1033	-0.01597	-0.03606
0.1464	-0.00819	-0.03163
0.1956	-0.00036	-0.02683
0.2500	0.00710	-0.02202
0.3087	0.01376	-0.01756
0.3706	0.01923	-0.01375
0.4347	0.02318	-0.01084
0.5000	0.02534	-0.00903
0.5653	0.02559	-0.00841
0.6294	0.02377	-0.00904
0.6913	0.01988	-0.01092
0.7500	0.01402	-0.01402
0.8044	0.00626	-0.01838
0.8536	-0.00304	-0.02386
0.8967	-0.01298	-0.02984
0.9330	-0.02234	-0.03539
0.9619	-0.03009	-0.03965
0.9830	-0.03572	-0.04258
0.9957	-0.03906	-0.04435
1.0000	-0.04112	-0.04343

Table A-7. Rotor section shape, 80% span.

s/c	h/c Back	h/c Face
0.0000	-0.04028	-0.04028
0.0043	-0.03772	-0.04159
0.0170	-0.03405	-0.04166
0.0381	-0.02936	-0.04054
0.0670	-0.02382	-0.03841
0.1033	-0.01766	-0.03544
0.1464	-0.01111	-0.03186
0.1956	-0.00444	-0.02787
0.2500	0.00205	-0.02373
0.3087	0.00804	-0.01968
0.3706	0.01320	-0.01599
0.4347	0.01717	-0.01294
0.5000	0.01967	-0.01075
0.5653	0.02053	-0.00956
0.6294	0.01963	-0.00941
0.6913	0.01694	-0.01034
0.7500	0.01243	-0.01241
0.8044	0.00601	-0.01584
0.8536	-0.00215	-0.02066
0.8967	-0.01132	-0.02636
0.9330	-0.02029	-0.03199
0.9619	-0.02794	-0.03662
0.9830	-0.03360	-0.03990
0.9957	-0.03699	-0.04190
1.0000	-0.03896	-0.04120

Table A-8. Rotor section shape, 100% span.

s/c	h/c Back	h/c Face
0.0000	-0.03377	-0.03377
0.0043	-0.03145	-0.03527
0.0170	-0.02855	-0.03605
0.0381	-0.02511	-0.03613
0.0670	-0.02118	-0.03556
0.1033	-0.01684	-0.03437
0.1464	-0.01215	-0.03261
0.1956	-0.00724	-0.03034
0.2500	-0.00228	-0.02770
0.3087	0.00258	-0.02476
0.3706	0.00718	-0.02160
0.4347	0.01133	-0.01836
0.5000	0.01468	-0.01532
0.5653	0.01681	-0.01286
0.6294	0.01726	-0.01138
0.6913	0.01577	-0.01113
0.7500	0.01224	-0.01226
0.8044	0.00683	-0.01474
0.8536	-0.00002	-0.01830
0.8967	-0.00765	-0.02252
0.9330	-0.01528	-0.02686
0.9619	-0.02213	-0.03074
0.9830	-0.02732	-0.03367
0.9957	-0.03047	-0.03544
1.0000	-0.03234	-0.03485

STATOR GEOMETRY

Table A-9 lists the stator spanwise geometric characteristics. The stator reference line is located at x/R=1.53 relative to the upstream end of the rotor hub. Tables A-10 through A-15 contain selected section shapes. The spanwise data and blade sections are defined on the section generation curves, which are uniformly spaced between the hub and casing, and shown earlier in Figure 3.

Table A-9. Stator spanwise geometry.

span	c/D	t/c	t/D	Pitch (deg)	Skew (deg)	Rake/D
0.00	0.4000	0.0800	0.0320	114.70	0.000	0.0000
0.05	0.3997	0.0604	0.0241	114.26	0.290	0.0093
0.10	0.3988	0.0522	0.0208	113.84	0.938	0.0145
0.15	0.3973	0.0486	0.0193	113.44	1.790	0.0175
0.20	0.3952	0.0471	0.0186	113.06	2.778	0.0189
0.25	0.3926	0.0464	0.0182	112.69	3.864	0.0192
0.30	0.3894	0.0460	0.0179	112.33	5.027	0.0187
0.35	0.3856	0.0457	0.0176	111.97	6.250	0.0175
0.40	0.3814	0.0455	0.0173	111.61	7.524	0.0157
0.45	0.3767	0.0453	0.0171	111.24	8.840	0.0135
0.50	0.3714	0.0453	0.0168	110.85	10.192	0.0109
0.55	0.3658	0.0453	0.0166	110.42	11.576	0.0079
0.60	0.3597	0.0455	0.0164	109.91	12.987	0.0045
0.65	0.3533	0.0457	0.0161	109.21	14.424	0.0010
0.70	0.3467	0.0460	0.0159	108.23	15.882	-0.0029
0.75	0.3400	0.0464	0.0158	106.90	17.361	-0.0069
0.80	0.3336	0.0471	0.0157	105.16	18.858	-0.0112
0.85	0.3277	0.0486	0.0159	102.95	20.372	-0.0157
0.90	0.3232	0.0522	0.0169	100.23	21.901	-0.0203
0.95	0.3207	0.0604	0.0194	96.98	23.444	-0.0251
1.00	0.3200	0.0800	0.0256	93.20	25.000	-0.0300

Table A-10. Stator section shape, 0% span.

Back		Face	
s/c	h/c	s/c	h/c
0.0000	0.0854	0.0000	0.0854
0.0033	0.0795	0.0053	0.0895
0.0151	0.0721	0.0190	0.0917
0.0353	0.0633	0.0408	0.0921
0.0634	0.0532	0.0706	0.0908
0.0989	0.0419	0.1077	0.0878
0.1413	0.0296	0.1516	0.0831
0.1898	0.0164	0.2014	0.0770
0.2438	0.0029	0.2562	0.0695
0.3025	-0.0104	0.3148	0.0614
0.3649	-0.0226	0.3763	0.0533
0.4300	-0.0328	0.4394	0.0458
0.4969	-0.0399	0.5031	0.0399
0.5643	-0.0429	0.5663	0.0361
0.6309	-0.0412	0.6280	0.0350
0.6953	-0.0340	0.6874	0.0371
0.7559	-0.0214	0.7441	0.0423
0.8111	-0.0049	0.7977	0.0501
0.8601	0.0136	0.8470	0.0591
0.9024	0.0323	0.8910	0.0682
0.9374	0.0495	0.9286	0.0764
0.9650	0.0636	0.9589	0.0827
0.9850	0.0738	0.9810	0.0867
0.9969	0.0797	0.9945	0.0888
1.0000	0.0854	1.0000	0.0854

Table A-11. Stator section shape, 20% span.

Back		Face	
s/c	h/c	s/c	h/c
0.0000	0.0818	0.0000	0.0818
0.0034	0.0774	0.0052	0.0831
0.0154	0.0704	0.0187	0.0817
0.0357	0.0613	0.0404	0.0780
0.0642	0.0506	0.0698	0.0724
0.1002	0.0388	0.1065	0.0656
0.1431	0.0266	0.1498	0.0580
0.1923	0.0144	0.1989	0.0501
0.2469	0.0030	0.2531	0.0424
0.3059	-0.0071	0.3114	0.0354
0.3685	-0.0153	0.3727	0.0297
0.4334	-0.0209	0.4360	0.0256
0.4996	-0.0235	0.5004	0.0235
0.5659	-0.0229	0.5646	0.0237
0.6310	-0.0188	0.6278	0.0260
0.6938	-0.0113	0.6888	0.0305
0.7531	-0.0008	0.7469	0.0369
0.8077	0.0119	0.8010	0.0446
0.8568	0.0260	0.8503	0.0533
0.8996	0.0404	0.8938	0.0619
0.9353	0.0536	0.9307	0.0699
0.9636	0.0646	0.9603	0.0763
0.9841	0.0728	0.9818	0.0808
0.9965	0.0777	0.9950	0.0835
1.0000	0.0818	1.0000	0.0818

Table A-12. Stator section shape, 40% span.

Back		Face	
s/c	h/c	s/c	h/c
0.0000	0.0885	0.0000	0.0885
0.0032	0.0837	0.0054	0.0891
0.0151	0.0757	0.0190	0.0864
0.0354	0.0650	0.0408	0.0808
0.0638	0.0524	0.0702	0.0732
0.0999	0.0389	0.1068	0.0646
0.1429	0.0253	0.1500	0.0554
0.1922	0.0121	0.1991	0.0464
0.2469	0.0001	0.2531	0.0382
0.3061	-0.0099	0.3112	0.0312
0.3689	-0.0174	0.3723	0.0261
0.4340	-0.0218	0.4355	0.0232
0.5003	-0.0227	0.4997	0.0227
0.5666	-0.0201	0.5640	0.0248
0.6316	-0.0141	0.6272	0.0291
0.6942	-0.0050	0.6885	0.0353
0.7532	0.0066	0.7468	0.0430
0.8077	0.0198	0.8010	0.0515
0.8567	0.0339	0.8504	0.0603
0.8994	0.0478	0.8939	0.0689
0.9352	0.0607	0.9308	0.0767
0.9636	0.0715	0.9603	0.0831
0.9841	0.0795	0.9818	0.0876
0.9965	0.0844	0.9949	0.0903
1.0000	0.0885	1.0000	0.0885

Table A-13. Stator section shape, 60% span.

Back		Face	
s/c	h/c	s/c	h/c
0.0000	0.0977	0.0000	0.0977
0.0030	0.0924	0.0056	0.0976
0.0148	0.0830	0.0193	0.0935
0.0350	0.0705	0.0412	0.0860
0.0633	0.0559	0.0706	0.0765
0.0994	0.0406	0.1072	0.0660
0.1425	0.0253	0.1504	0.0553
0.1919	0.0109	0.1994	0.0451
0.2467	-0.0019	0.2533	0.0360
0.3061	-0.0124	0.3112	0.0288
0.3691	-0.0196	0.3721	0.0239
0.4344	-0.0231	0.4351	0.0218
0.5008	-0.0227	0.4992	0.0227
0.5672	-0.0183	0.5633	0.0265
0.6323	-0.0103	0.6265	0.0327
0.6948	0.0008	0.6879	0.0409
0.7537	0.0140	0.7463	0.0503
0.8080	0.0284	0.8008	0.0600
0.8568	0.0432	0.8503	0.0697
0.8995	0.0575	0.8938	0.0787
0.9353	0.0704	0.9308	0.0866
0.9636	0.0811	0.9603	0.0929
0.9841	0.0889	0.9818	0.0973
0.9965	0.0936	0.9949	0.0998
1.0000	0.0977	1.0000	0.0977

Table A-14. Stator section shape, 80% span.

Back		Face	
s/c	h/c	s/c	h/c
0.0000	0.1148	0.0000	0.1148
0.0028	0.1086	0.0058	0.1138
0.0144	0.0975	0.0197	0.1079
0.0344	0.0825	0.0417	0.0981
0.0627	0.0650	0.0713	0.0859
0.0987	0.0469	0.1079	0.0728
0.1418	0.0292	0.1511	0.0599
0.1912	0.0126	0.2000	0.0478
0.2461	-0.0019	0.2539	0.0372
0.3057	-0.0137	0.3116	0.0288
0.3690	-0.0215	0.3722	0.0235
0.4346	-0.0248	0.4349	0.0217
0.5013	-0.0235	0.4987	0.0235
0.5678	-0.0177	0.5627	0.0286
0.6330	-0.0077	0.6258	0.0366
0.6956	0.0056	0.6871	0.0469
0.7545	0.0213	0.7455	0.0585
0.8087	0.0382	0.8000	0.0707
0.8575	0.0552	0.8496	0.0825
0.9000	0.0714	0.8934	0.0933
0.9356	0.0858	0.9305	0.1025
0.9638	0.0974	0.9601	0.1097
0.9842	0.1057	0.9817	0.1145
0.9965	0.1104	0.9949	0.1171
1.0000	0.1148	1.0000	0.1148

Table A-15. Stator section shape, 100% span.

Back		Face	
s/c	h/c	s/c	h/c
0.0000	0.1010	0.0000	0.1010
0.0014	0.0917	0.0072	0.1000
0.0118	0.0754	0.0223	0.0924
0.0308	0.0541	0.0454	0.0797
0.0584	0.0302	0.0755	0.0645
0.0945	0.0065	0.1121	0.0499
0.1384	-0.0148	0.1545	0.0373
0.1893	-0.0322	0.2019	0.0281
0.2463	-0.0445	0.2537	0.0229
0.3078	-0.0511	0.3096	0.0218
0.3725	-0.0521	0.3687	0.0245
0.4391	-0.0479	0.4304	0.0308
0.5057	-0.0396	0.4943	0.0396
0.5713	-0.0292	0.5593	0.0490
0.6355	-0.0176	0.6233	0.0578
0.6975	-0.0045	0.6851	0.0660
0.7559	0.0096	0.7441	0.0736
0.8098	0.0241	0.7990	0.0802
0.8585	0.0386	0.8486	0.0858
0.9012	0.0533	0.8922	0.0910
0.9369	0.0674	0.9292	0.0962
0.9649	0.0797	0.9590	0.1008
0.9851	0.0890	0.9808	0.1041
0.9970	0.0945	0.9944	0.1058
1.0000	0.1010	1.0000	0.1010

REFERENCES

1. Kerwin, J. E., et. al., "A Coupled Viscous/Potential Flow Design Method for Wake-Adapted Multi-Stage, Ducted Propulsors Using Generalized Geometry," SNAME Transactions, 1994.
2. Drela, M. and Giles, M., "Conservative Streamtube Solution of Steady-State Euler Equations," Technical Report CFDL-TR-83-6, Department of Aeronautics and Astronautics, Massachusetts Institute of Technology, November 1983.
3. Renick, D.H., "An Analysis Procedure for Advanced Propulsor Design," Masters Thesis, Ocean Engineering Department, Massachusetts Institute of Technology, May 1999.
4. Kerwin, J.E., Michael, T.J., and Neely, S.K., "Improved Algorithms for the Design/Analysis of Multi-Component Complex Propulsors," SNAME Propellers and Shafting Symposium, September 2006.
5. Menter, F.R., "Zonal Two Equation k-ω Turbulence Models for Aerodynamic Flows," AIAA Paper 93-2906, 1993.
6. "Fluent 6.3 User's Guide," Fluent, Inc., September 2006.
7. Neely, S.K., "Non-Cylindrical Blade Geometry Definition," SNAME Propellers and Shafting Symposium, September 1997.
8. Neely, S. K., "Application of NURBS Surfaces for Propeller Geometry," Proceedings of the 25th American Towing Tank Conference, September 1998.
9. Brewton, S., Gowing, S., and Gorksi, J., "Performance Predictions of a Waterjet Rotor and Rotor/Stator Combination Using RANS Calculations," 26th Symposium on Naval Hydrodynamics, September 2006.
10. Becnel, A. and Wheatley, S., "Development of a High Speed Sealift Waterjet Propulsion System," CDI Marine Company, Systems Development Division, Report number 748-9, September 2003.
11. Wislicenus, G.F., "Fluid Mechanics of Turbomachinery," McGraw-Hill Book Company, Inc, 1947.
12. Wu, H., et. al., "Cavitation in the Tip Region of the Rotor Blades within a Waterjet Pump," Proceedings of FEDSM2008, Fluids Engineering Conference 2008.
13. Kinas, S.A., et. al., "Prediction of Cavitating Waterjet Propulsor Performance Using a Boundary Element Method," 9th International Conference on Numerical Ship Hydrodynamics, August 2007.

(THIS PAGE INTENTIONALLY LEFT BLANK)

INITIAL DISTRIBUTION

EXTERNAL DISTRIBUTION

ORG.	NAME (Copies)
Johns Hopkins University	
	J. Katz
Massachusetts Institute of Technology	
	J. Kerwin
Naval Sea Systems Command	
	J. Schumann
Office of Naval Research	
331	K.-H. Kim
Pennsylvania State University, Applied Research Laboratory	
	E. Paterson
Princeton University	
	Y.-L. Young
University of Iowa	
	F. Stern
University of Texas, Austin	
	S. Kinnas
DTIC	(1)

CENTER DISTRIBUTION

CODE	NAME (Copies)
5030	S. Jessup
5060	D. Walden
5500	A. Becnel
5800	C. Chesnakas
5800	M. Donnelly
5800	T. Michael
5800	S. Schroeder
5800	File (2)
3452	Library


UNITED STATES NAVY
SURFACE WARFARE CENTER